NRL Report 9155

Images of the Geopotential

PETER J. MELVIN

Naval Center for Space Technology

November 14, 1988

SECURITY CLASSIFICATION OF THIS PAGE

REPORT DOCUMENTATION PAGE

Form Approved
OMB No 0704-0188

1a REPORT SECURITY CLASSIFICATION UNCLASSIFIED	1b RESTRICTIVE MARKINGS
2a SECURITY CLASSIFICATION AUTHORITY	3 DISTRIBUTION / AVAILABILITY OF REPORT Approved for public release; distribution unlimited.
2b DECLASSIFICATION / DOWNGRADING SCHEDULE	
4 PERFORMING ORGANIZATION REPORT NUMBER(S) NRL Report 9155	5 MONITORING ORGANIZATION REPORT NUMBER(S)
6a NAME OF PERFORMING ORGANIZATION Naval Research Laboratory 6b OFFICE SYMBOL (If applicable) Code 8103	7a NAME OF MONITORING ORGANIZATION
6c ADDRESS (City, State, and ZIP Code) Washington, DC 20375-5000	7b ADDRESS (City, State, and ZIP Code)
8a NAME OF FUNDING / SPONSORING ORGANIZATION Office of Naval Research 8b OFFICE SYMBOL (If applicable)	9 PROCUREMENT INSTRUMENT IDENTIFICATION NUMBER
8c ADDRESS (City, State, and ZIP Code) Arlington, VA 22217	10 SOURCE OF FUNDING NUMBERS PROGRAM ELEMENT NO / PROJECT NO / TASK NO / WORK UNIT ACCESSION NO DN380-020
11 TITLE (Include Security Classification) Images of the Geopotential	
12 PERSONAL AUTHOR(S) Melvin, P.J.	
13a TYPE OF REPORT Final 13b TIME COVERED FROM _____ TO _____	14 DATE OF REPORT (Year, Month, Day) 1988 November 14 15 PAGE COUNT 57
16 SUPPLEMENTARY NOTATION Original copies available from the Commanding Officer, Naval Research Laboratory, Code 2628, Washington, DC 20375-5000.	

17 COSATI CODES			18 SUBJECT TERMS (Continue on reverse if necessary and identify by block number)		
FIELD	GROUP	SUB-GROUP	Geopotential	Geodesy	GEM-L2
			Spherical harmonics	RAPP81	WGS84
			Gravity	OSU86F	

19 ABSTRACT (Continue on reverse if necessary and identify by block number)

To compare the detailed differences in geopotential models, a series of graphics of the undulation of the geoid, anomalous gravity components, and gravity gradient components for GEM-L2, WGS84, RAPP81, and OSU86F is presented as complementary contour maps, gray scale images, and spherical projections.

20 DISTRIBUTION / AVAILABILITY OF ABSTRACT ☒ UNCLASSIFIED/UNLIMITED ☐ SAME AS RPT ☐ DTIC USERS	21 ABSTRACT SECURITY CLASSIFICATION UNCLASSIFIED
22a NAME OF RESPONSIBLE INDIVIDUAL Peter J. Melvin	22b TELEPHONE (Include Area Code) (202) 767-1899 22c OFFICE SYMBOL Code 8103

DD Form 1473, JUN 86 *Previous editions are obsolete.* SECURITY CLASSIFICATION OF THIS PAGE

CONTENTS

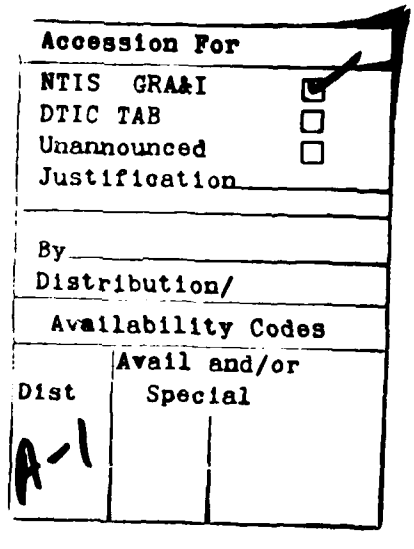

IMAGES OF THE GEOPOTENTIAL

INTRODUCTION

This report is the author's fourth collection of graphics of fields computed from spherical harmonic, geopotential models. The first collection, Ref. 1, presents the undulation of the geoid, anomalous gravitational force components, and gravity gradient components of the 36th order potential GEM10B of Lerch et al. [2]. (Reference 3 is not counted because only the equatorial, longitudinal undulation is plotted at synchronous altitude for GEM 9 of Lerch et al. [4]). The second collection, Ref. 5, presents the RAPP81 undulation of the geoid of Rapp [6] in equal angular and transverse Mercator projections. Reference 7 presents 11 contour maps of RAPP81 for the undulation of the geoid, the three anomalous gravity components, and two gravity gradient components. Except for the undulation of the geoid where line weights are used, it was necessary in Ref. 7 to separate the contour maps into positive and negative parts to quantify the contour levels.

With the 180th and higher order models, the problem arises of representing large amounts of information on a single piece of paper of a reasonable size, say 8.5 × 11 in. As mentioned in Ref. 5, a series of 18 × 36 in. maps were produced, but their size makes reproduction unwieldy. For awhile it was thought that the doubling of graphics could be eliminated with the "complementary contour images" presented here, where sign is distinguished by drawing the contour lines either on a white or a black background. The complementary contour technique is adequate for the undulation of the geoid at all orders and for the other fields up to order 180, but it proved to be inadequate for Rapp's 1/8° gravity anomaly, described in Refs. 8 and 9, and the 360th order force and gradient fields of OSU86F described by Rapp and Cruz in Ref. 10.

This report presents five series of graphics produced at the Naval Research Laboratory (NRL) during the period from the spring of 1986 to the fall of 1987. The first series is complementary contour images of all 10 fields of RAPP81. The second series is of Rapp's 1° and 1/8° gridded data. The third series is gray scale representations of OSU86F. The fourth series is spherical projections of the undulation of the geoid of OSU86F. The fifth series is for the comparison of three independently produced geopotential models at low order.

A SECOND ATLAS OF RAPP'S 180TH ORDER GEOPOTENTIAL

A "complementary contour image" is a graphic that is created by contouring positive values with black lines on a white background and negative values with white lines on a black background. That is, the contour map of the negative values is formed by the logical complement of the bits used to form the contour map of the positive values. The development of the complementary contour image means that the separation of positive and negative contours into two maps used in Ref. 7 to gain partial quantitative information from unlabeled contours is not necessary. Complete quantitative information is not gained, however, because counting contours works only in regions of a monotone gradient from the zero level that separates the white and black backgrounds. Further information is

Manuscript approved August 12, 1988.

needed to decide whether a closed contour represents a bump up or a bump down in the field. In this report, maps of RAPP81 are again presented, but this time with all 10 fields available from the algorithm of Ref. 7.

The complementary contour images are constructed in several steps. Individual bit images are formed for the positive and negative contours. A third bit image mask is then created by evaluating (or interpolating) the field at each pixel and setting the pixel according to whether the field value is positive or negative. The three images are then logically combined along with a fourth of the continental outlines to produce the graphics.

Figure 1(a) is the undulation of the geoid with a 2-m contour interval; Fig. 1(b) is the gravity disturbance with a 10-mGal contour interval. The gravity disturbance is the radial derivative of the potential evaluated on the ellipsoid with normal gravity values subtracted from the even zonal harmonics. Figures 2(a) and 2(b) are the longitude and latitude gravity disturbances or deflections with a contour interval of 10 mGal. Reference 11 shows that when a high band-pass filter is applied to the intersatellite range rate for a pair of polar-orbiting, coplanar satellites, the spectrum of the perturbations looks like that of the latitude gravity disturbance. That is, for frequencies above twice per orbit, intersatellite range rate in essence maps the along-track deflection of the vertical; for a high inclination satellite, this looks like the latitude deflection.

The next six maps show components of the anomalous gravity gradient tensor with a contour interval of two Eötvös units. Figure 3(a) is the radial-longitude component; Fig. 3(b) is the radial-latitude component. When rotated into the Orlov plane of Ref. 12, Ref. 13 shows that these components force the librations of a gravity gradient pendulum on a polar orbit. Figure 4(a) plots the second radial derivative of the geopotential; Fig. 4(b) plots the longitude-longitude component. Figure 5(a) maps the latitude-longitude component. It is this component (latitude-longitude) that most accentuates any satellite ephemeris error that may be carried into the geopotential model from the radar altimetry data. Figure 5(b) maps the latitude-latitude gravity gradient component that by Laplace's equation gives redundant information.

Figures 6(a) and 6(b) are transverse Mercator projections of the undulation of the geoid and the radial gravity disturbance to show polar behavior. A similar map appears in Ref. 14. In a personal communication, Peter Vogt of the Acoustics Division of NRL suggested the central longitude of 64° in these projections because it most equally divides the Atlantic Ocean.

A second reason for again presenting RAPP81 is to have a uniform method of comparison with WGS84 which, besides Rapp, is the only other source known to the author for a high quality, high order geopotential model. A program called BLINK was developed by the author and Matthew Singer at NRL to compare the bit images presented here on the Hewlett-Packard Integral Personal Computer (HP IPC). Only 16K-byte windows are available on the 500K-byte maps, but the software scrolls through the images and simultaneously or selectively compares up to five maps on the HP IPC screen. The reader can get a general idea of this comparison by flipping the pages of this report, but the really fine details and gradations need BLINK. The gravity anomaly of RAPP81 is contoured in Ref. 15.

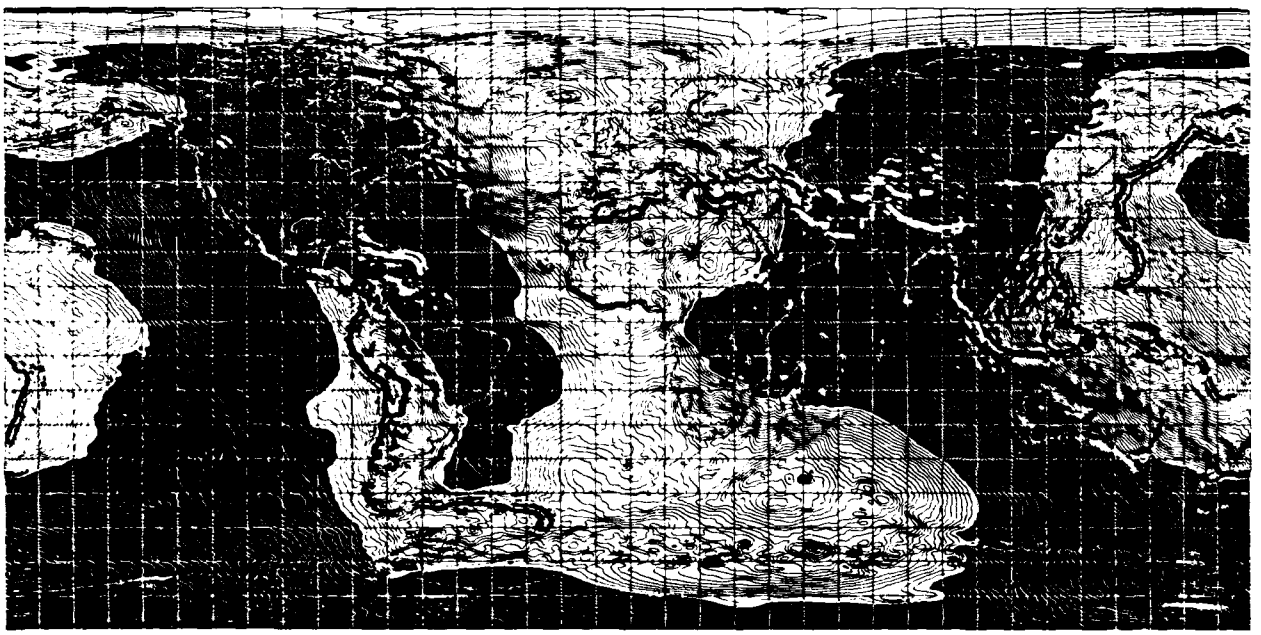

a. Undulation of the geoid

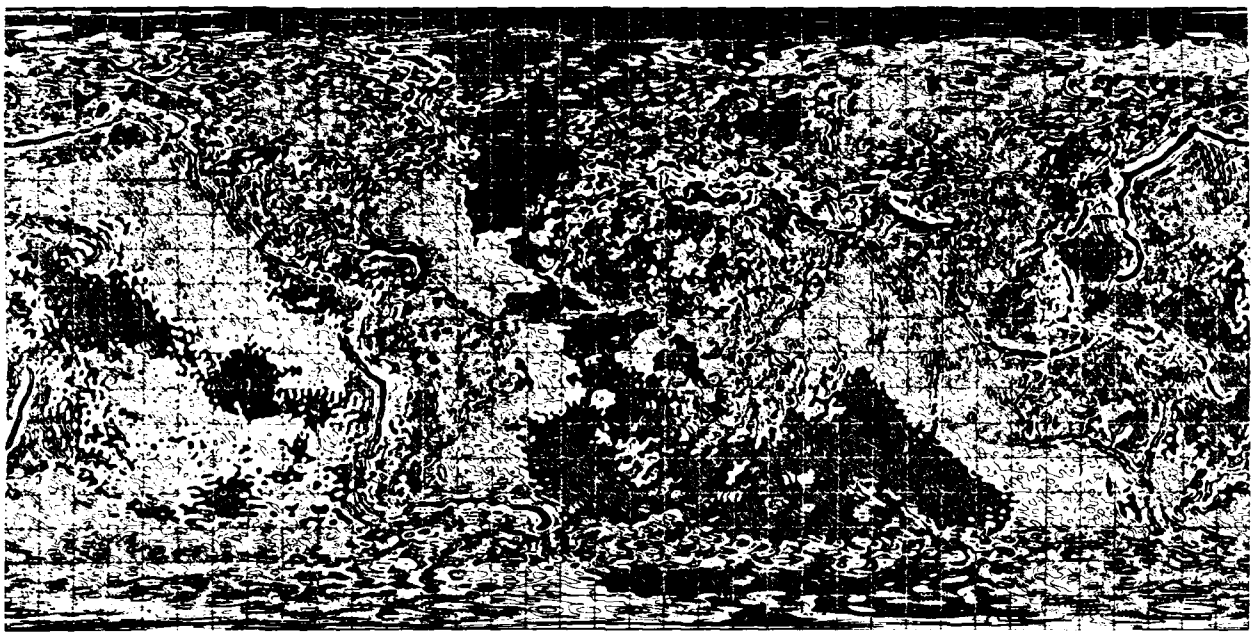

b. Gravity disturbance

Fig. 1 — RAPP81, 180th order geopotential model

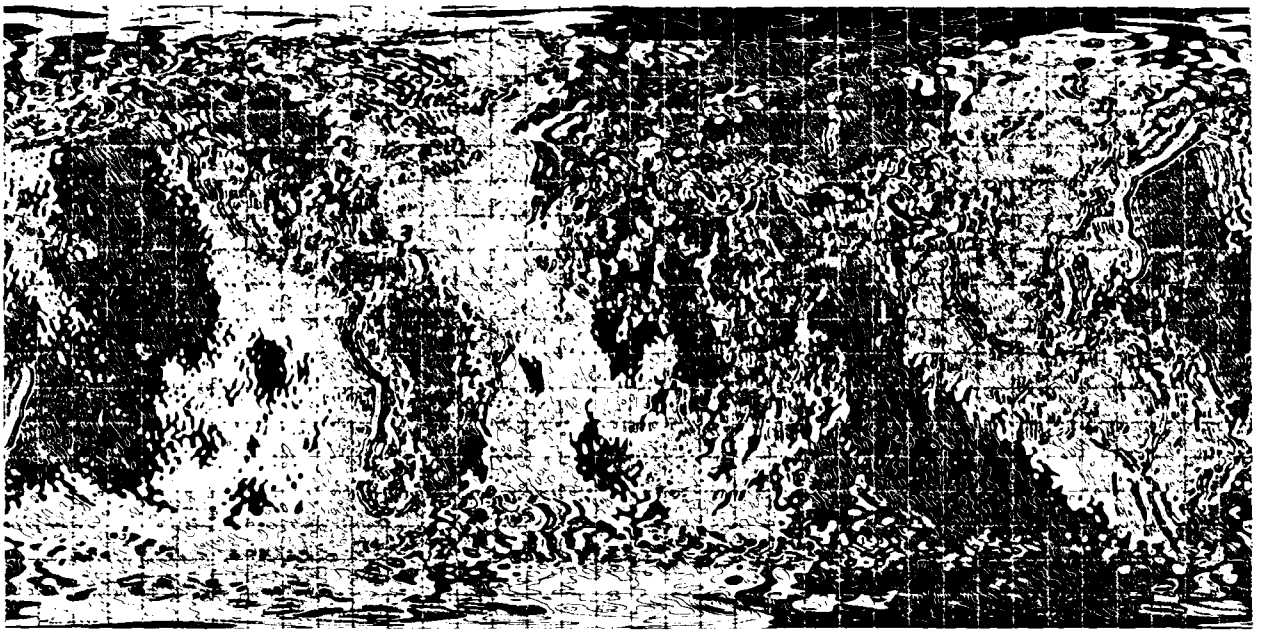

a. Longitude disturbance

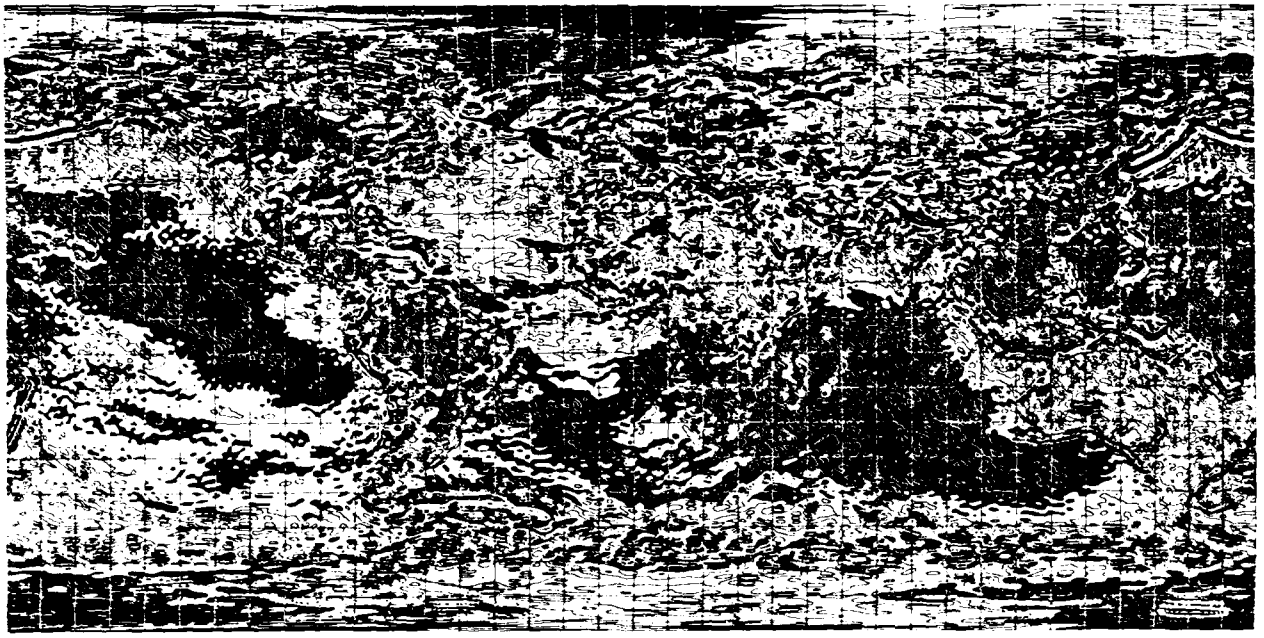

b. Latitude disturbance

Fig. 2 — RAPP81, 180th order geopotential model

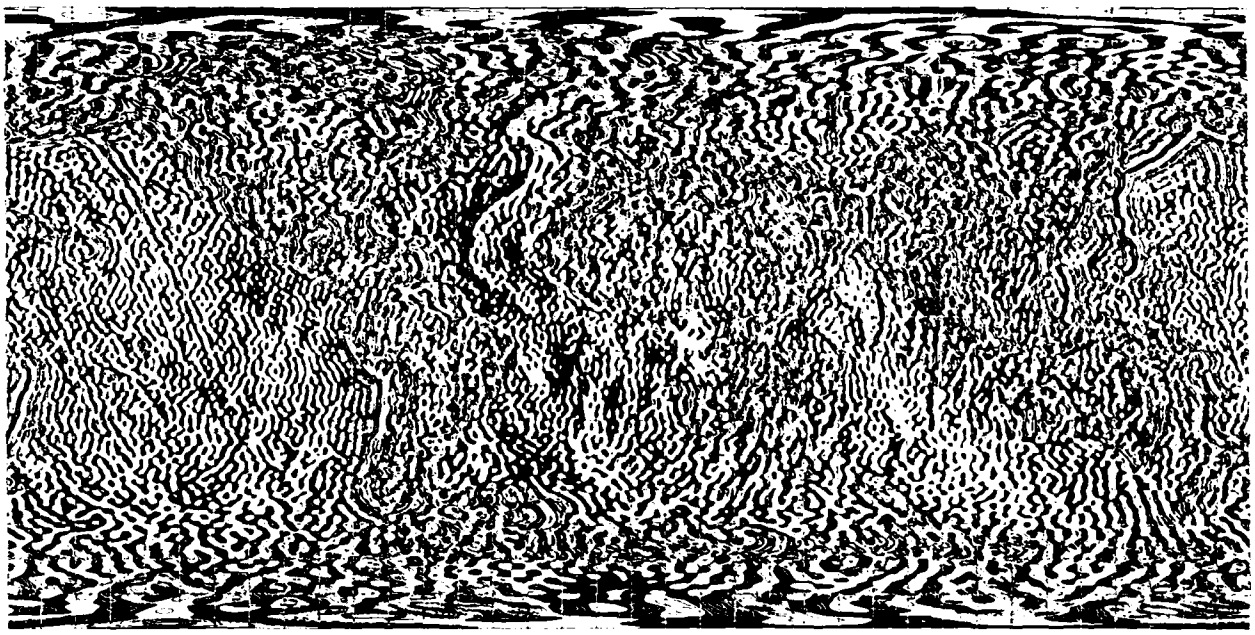

a. Anomalous radial-longitude gravity gradient

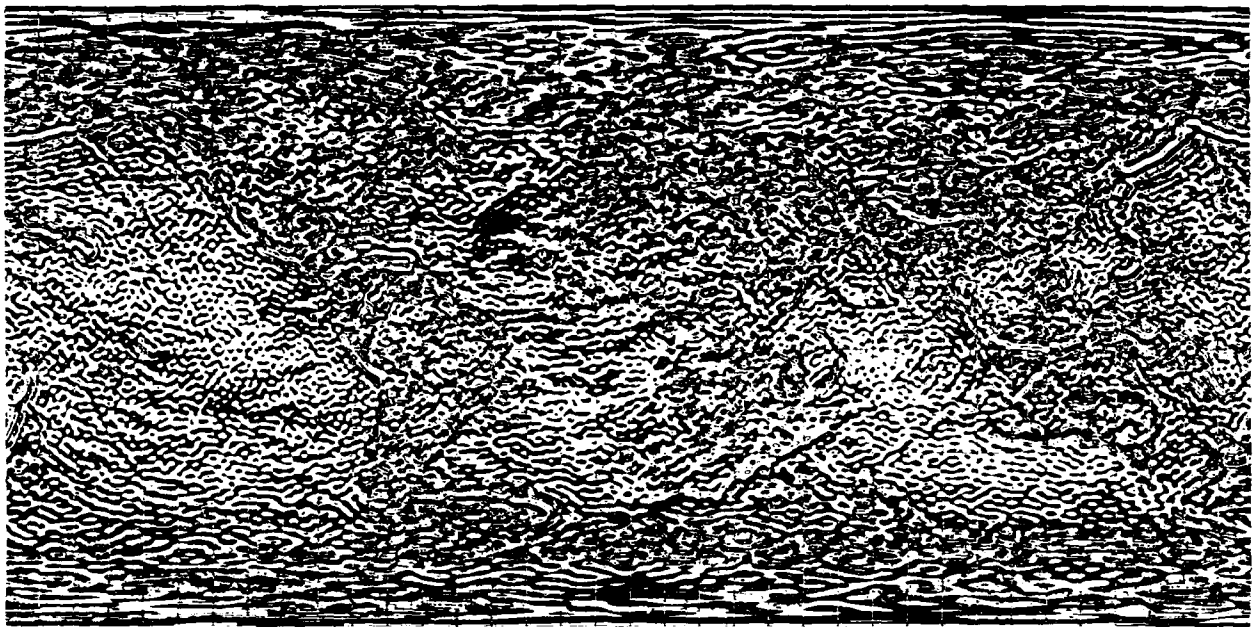

b. Anomalous radial-latitude gravity gradient

Fig. 3 — RAPP81, 180th order geopotential model

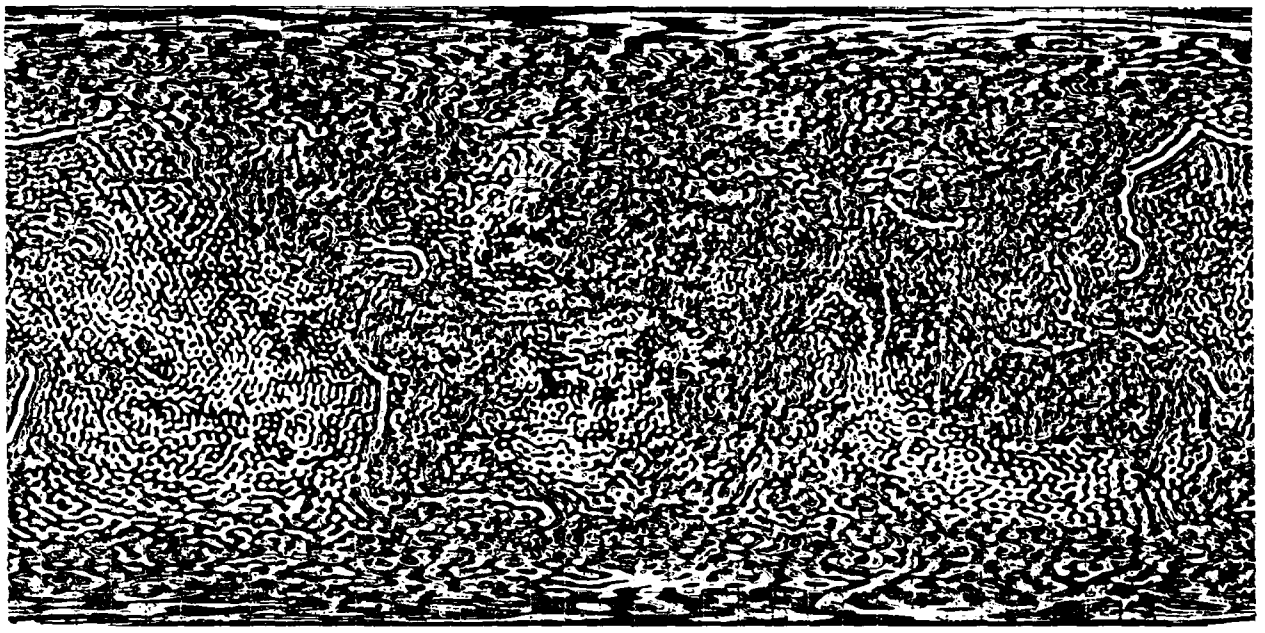

a. Anomalous radial-radial gravity gradient

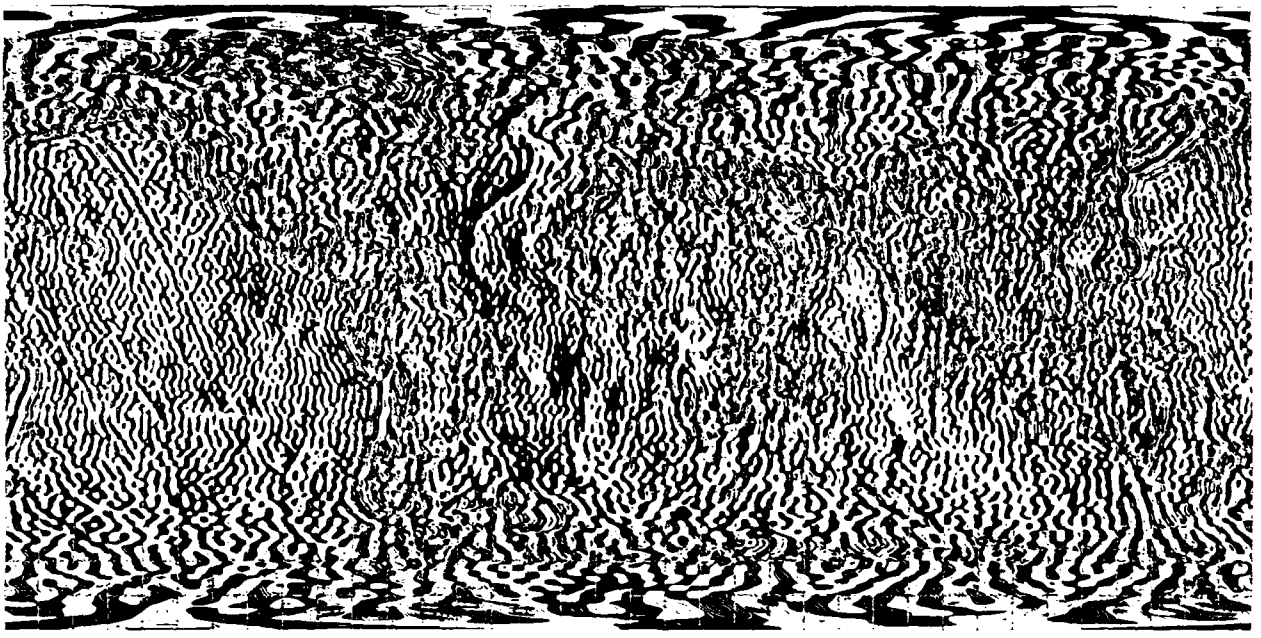

b. Anomalous longitude-longitude gravity gradient

Fig. 4 — RAPP81, 180th order geopotential model

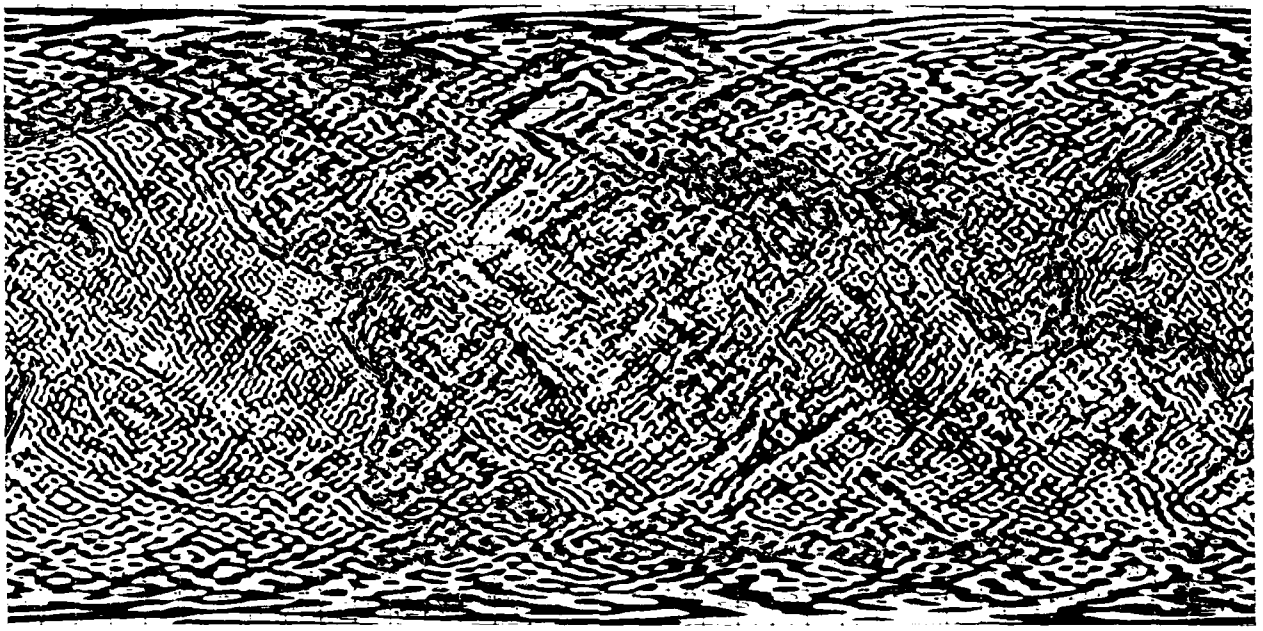

a. Anomalous longitude-latitude gravity gradient

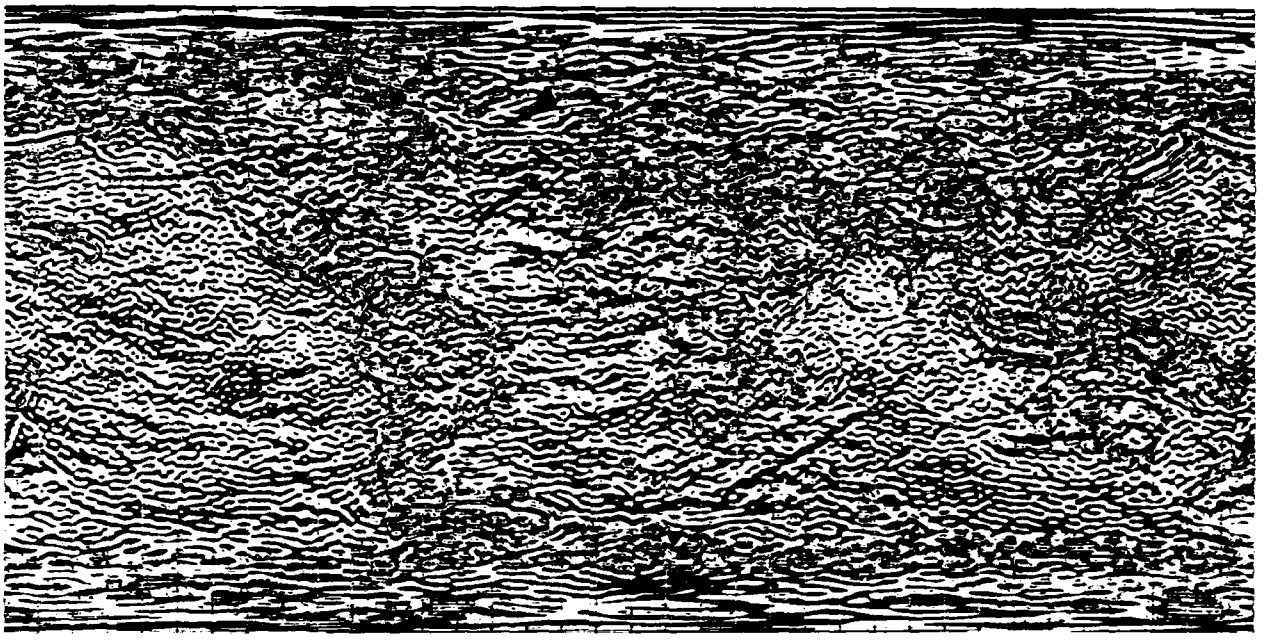

b. Anomalous latitude-latitude gravity gradient

Fig. 5 — RAPP81, 180th order geopotential model

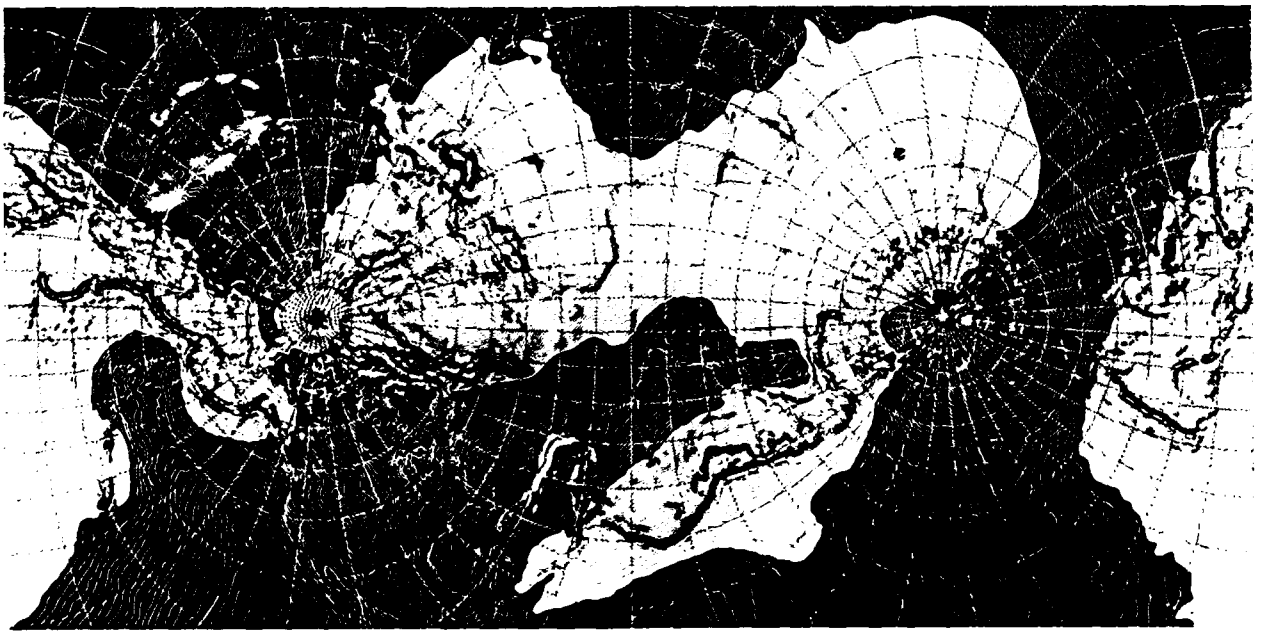

a. Undulation of the geoid

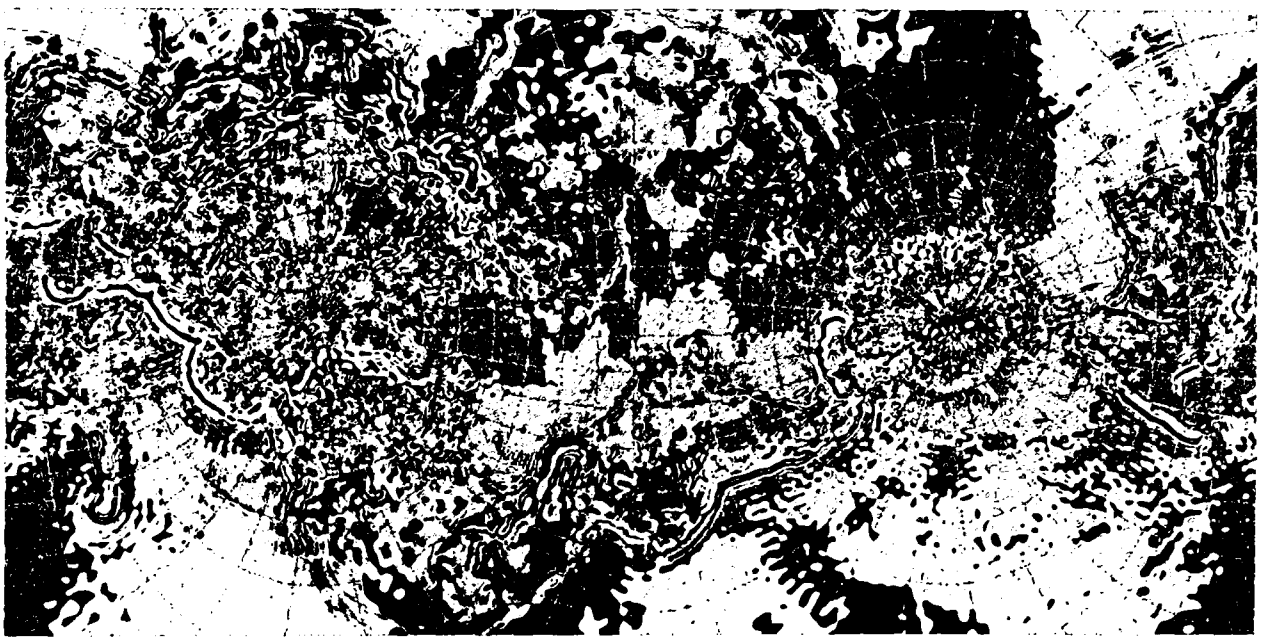

b. Gravity disturbance

Fig. 6 — RAPP81, 180th order geopotential model, transverse Mercator projection

RAPP'S GRIDDED DATA SETS

The next series of graphics is Rapp's 1° averages and the 1/8° values of sea surface heights and gravity anomalies described in Refs. 8 and 9. Figure 7 shows the 1° data. In Fig. 7(a) the sea surface heights are presented as a complementary contour image with a contour interval of 2 m. In Fig. 7(b) the gravity anomaly is plotted with a 10-mGal contour. Figures 8, 9(b), and 10 show the 1/8° data. In Fig. 8(a), the 1/8° sea surface is contoured with a 2-m interval. By flipping between Figs. 7(a) and 8(a), the contours shift at an amplitude that is much larger than the shift that might be expected. A linear interpolator is used to adjust for the differences in gridding between Rapp's data and that required for the images and is used also in conjunction with a 1/2° evaluation grid for the spherical harmonic models.

Figure 8(b) presents only the positive and negative mask for the gravity anomalies. It is a disappointment that although the complementary contour image is quite useful in all of the figures before this, there is so much information that contouring the 1/8° data turns into visual noise. This can be seen from the full complementary contour image of the 1/8° anomalies contoured at 10 mGal in Fig. 9(b). Figure 9(a) is the complementary contour image of the undulation of the geoid for OSU86F; it is presented at this location to provide easy comparison with the other undulation maps.

The continental data used to fill in the 1/8° grid is of particular interest because it is from RAPP81. It gives the reader the opportunity to see the differences over large areas between Rapp's and the author's evaluator. With BLINK, even smaller differences can be seen in the undulations of the geoid. This leads to understanding the subtle differences between Brun's formula for the undulation used by Rapp and Eq. (2.10c) of Ref. 1 or the unnumbered formula in Ref. 7. "BLINKing" the other field shows the difference between the gravity anomaly and the gravity disturbance. The sign difference between Rapp and the author is convention. It is customary to count a gravity anomaly as positive if it increases the acceleration of gravity. On the other hand, a positive gravity disturbance acts outward to decrease the acceleration of gravity.

In Figs. 10(a) and 10(b), the 1/8° data sets are this time represented with a gray scale described in the next section. Although not presented here, a gray scale image was also generated by use of the synthetic aperture radar image processing facilities of the Radar Division at NRL. Even though the results were of a better quality than shown in Fig. 10, the process as a whole was not satisfactory because of the time required to iterate on something as simple as the contrast of the image. A grid of data values had to be written from the VAX to tape which was then taken to the Data General computer, and the image was formed on photographic film with an Optronics film recorder which then had to be developed and printed.

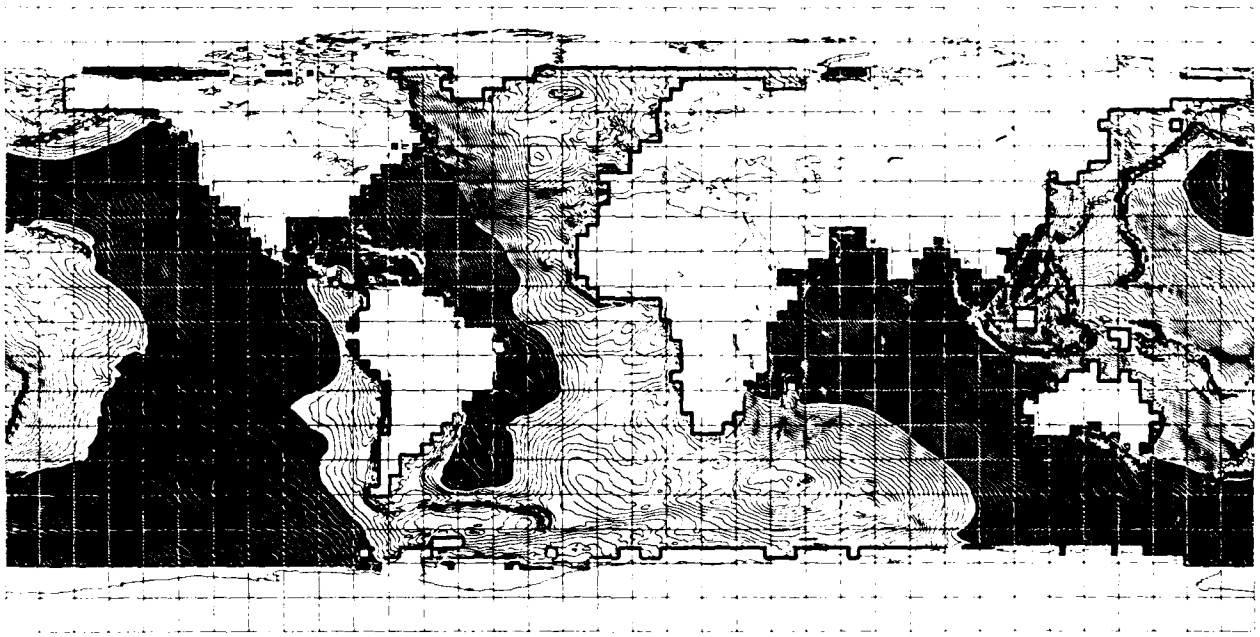

a. Sea surface heights

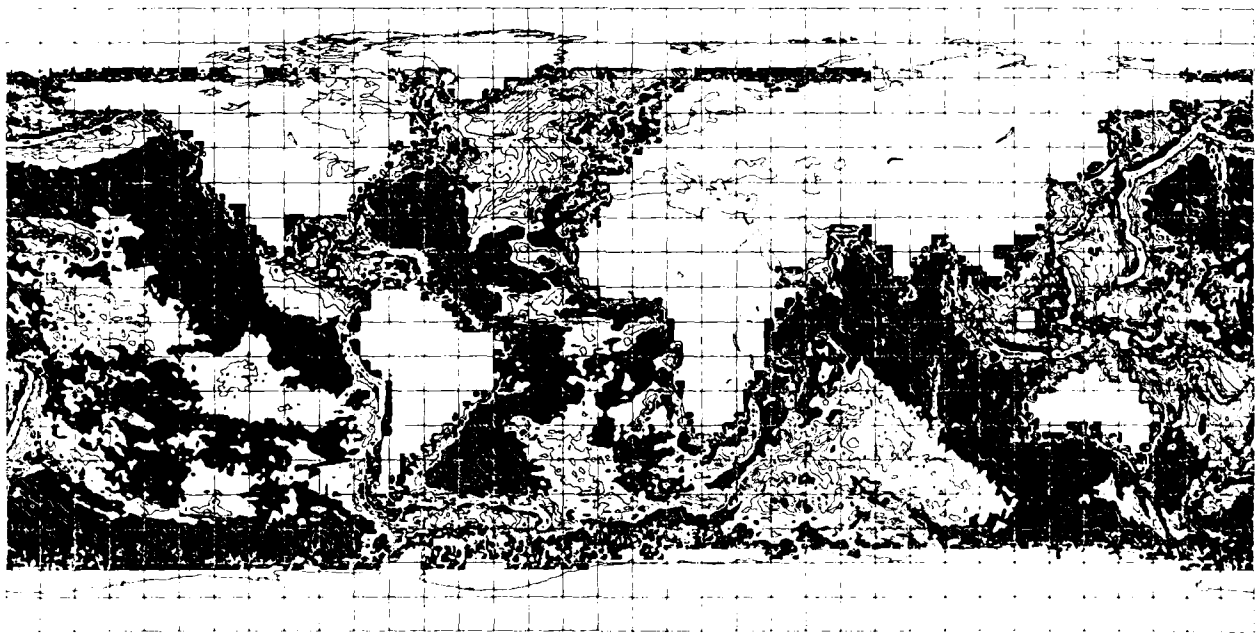

b. Gravity anomaly

Fig. 7 — 1° averages of GEOS-3/SEASAT altimetry

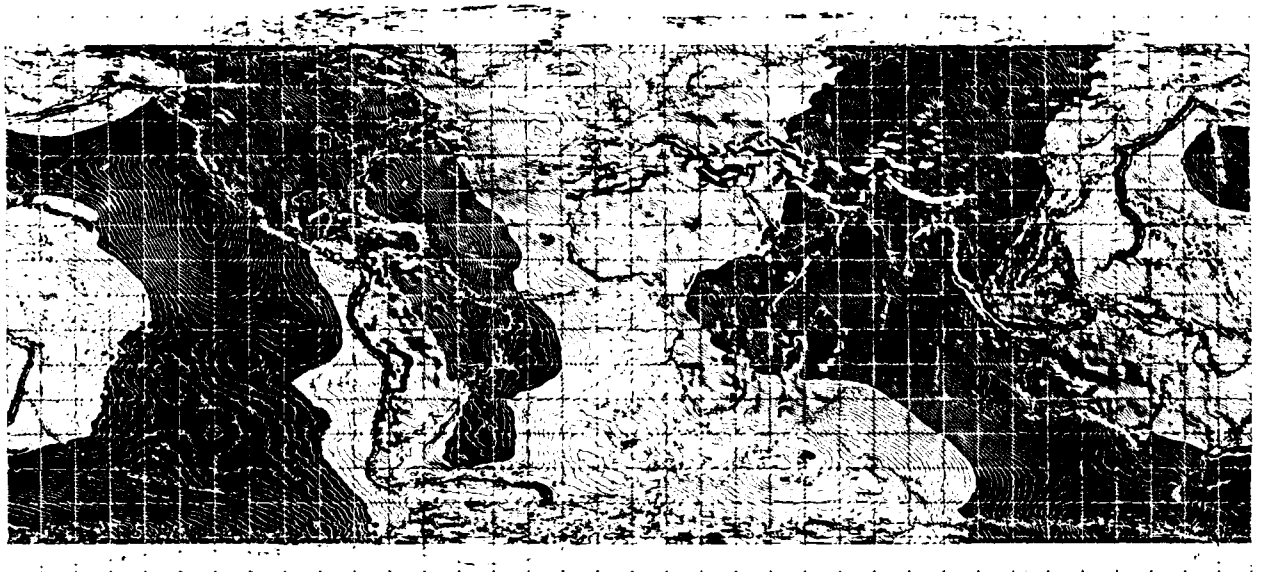

a. Sea surface heights

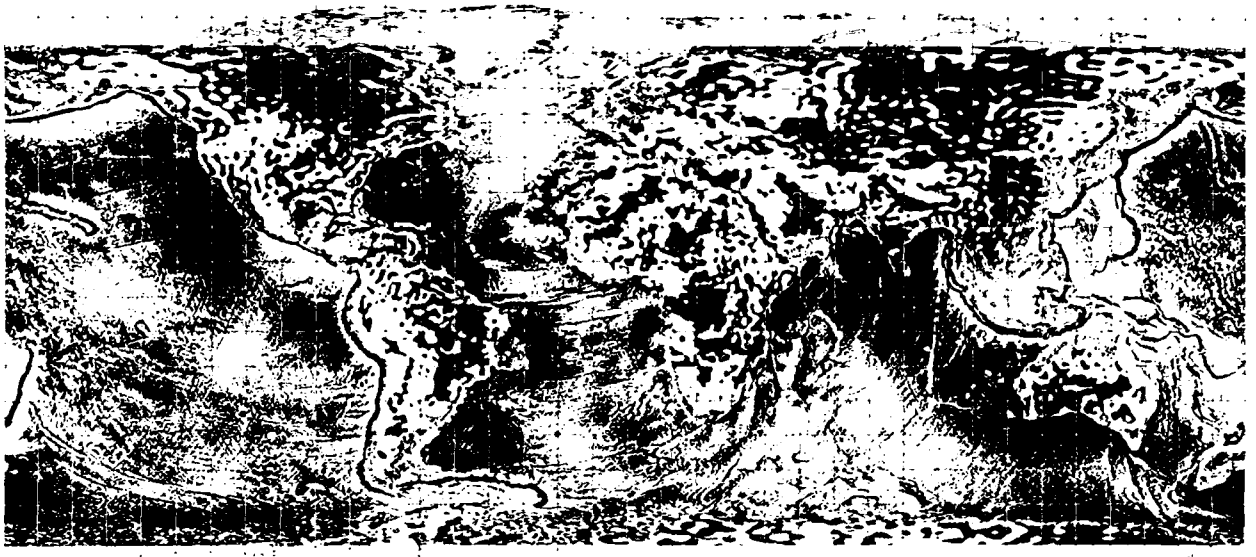

b. Gravity anomaly

Fig. 8 — 1/8° GEOS-3/SEASAT altimetry

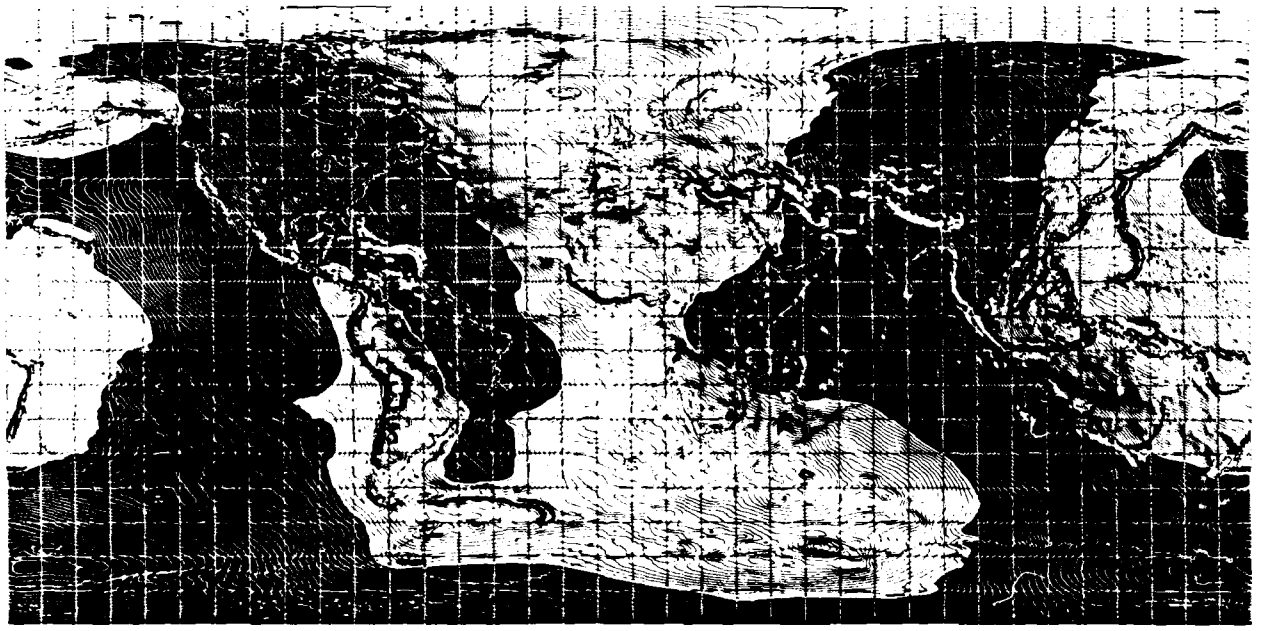

Fig. 9a — Undulation of geoid for OSU86F

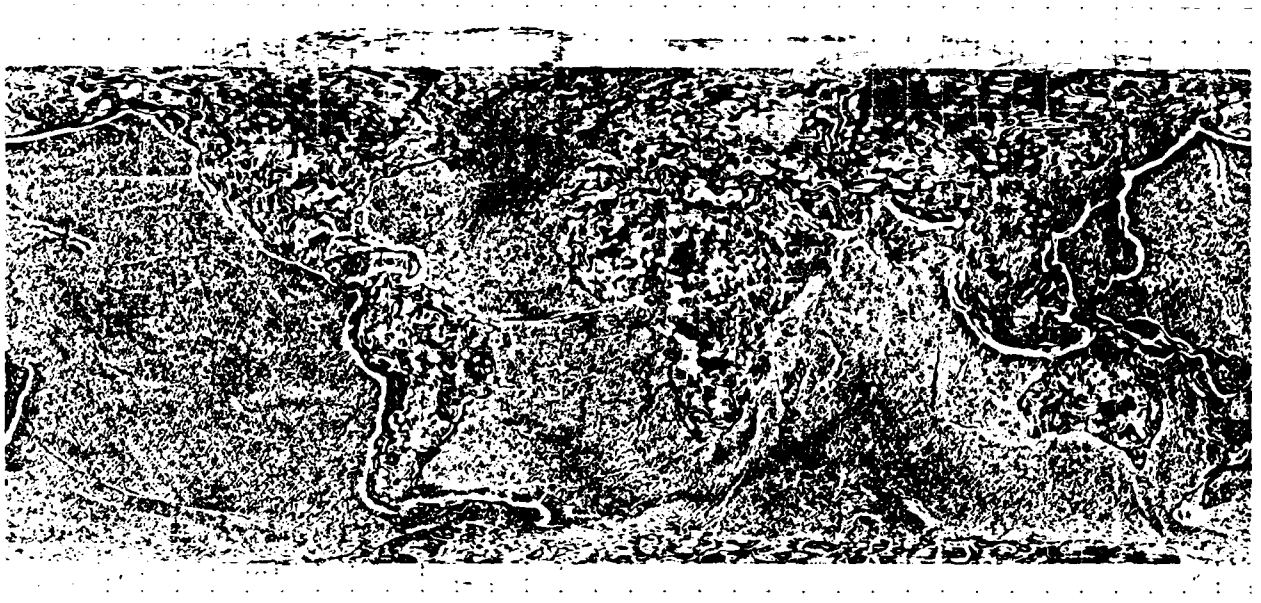

Fig. 9b — 1/8° GEOS-3/SEASAT gravity anomaly

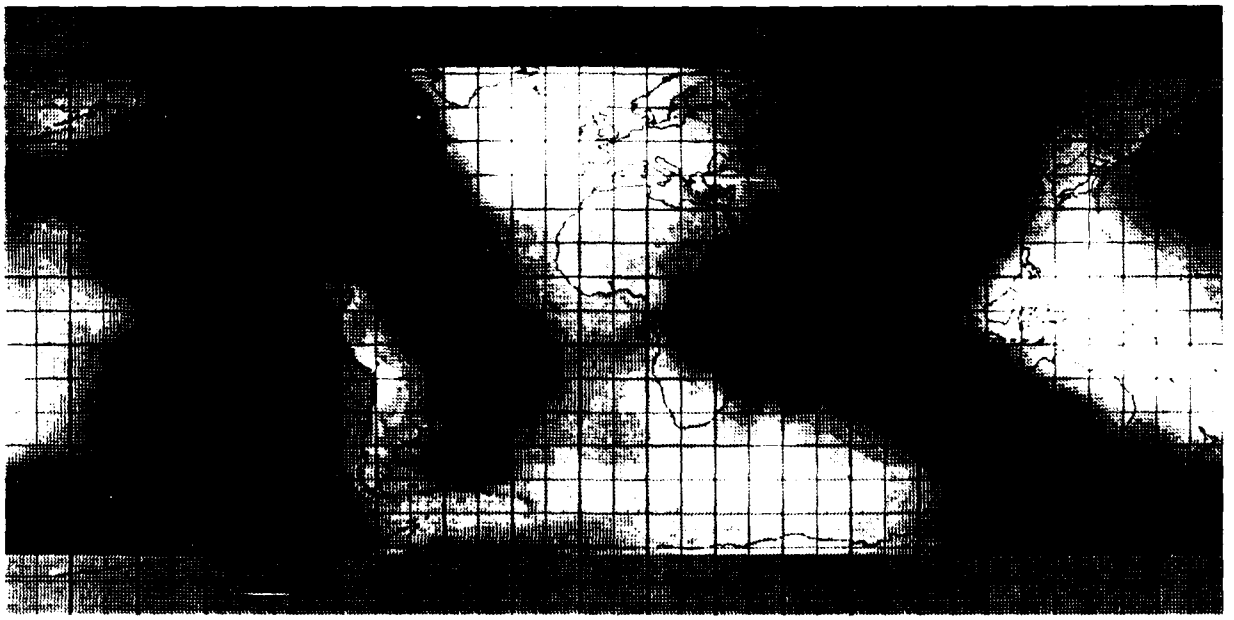

a. Sea surface heights

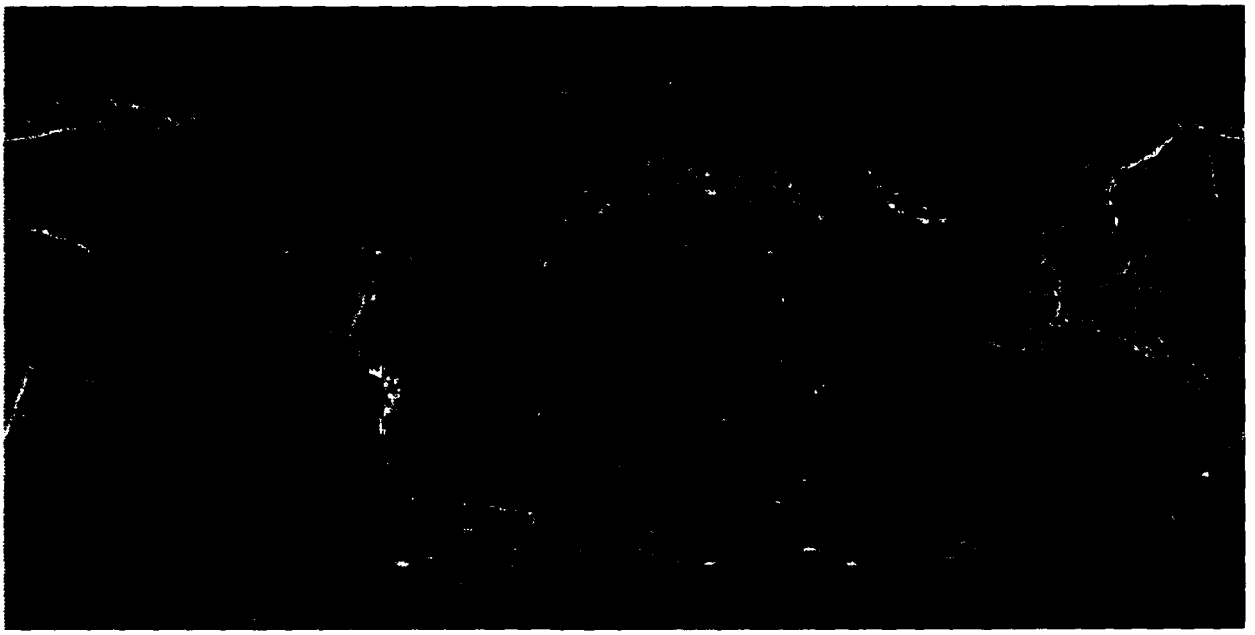

b. Gravity anomaly

Fig. 10 — 1/8° GEOS-3/SEASAT altimetry

GRAY SCALE IMAGES

For several years the author has attempted to devise an algorithm to make gray scale images on inexpensive dot matrix printing devices. Figures 11(a) and 11(b) show two images of the geoid that resulted from these experiments. Figure 11(a) shows 17 gray levels based on dots selected in a 4 × 4 pattern at regular grid intervals; Fig. 11(b) shows 65 gray levels. Both images are deemed unsatisfactory: Fig. 11(a) because the edges of the gray patterns abut, forming pseudo contours that detract from the gray level effect; Fig. 11(b) because it does not form an integrated image. Other experiments were performed in which the pattern of dots was chosen randomly each time, but the result was like a photograph with extremely dense grain. In another experiment, all possible combinations of placing dots in a 2 × 2 grid were used to distinguish 17 values with five gray levels.

Reference 5 reports that satisfactory color images were made with expensive imaging tubes with very difficult software. Hard copy was available only by photographing the screen. Some experiments were made with shaded relief, but these were unsatisfactory because the technique emphasizes the slopes of the surface which is in essence the same as taking a derivative. That is, the intensities of shaded relief of the geoid essentially show the deflections of the vertical.

Although the HP Laser Jet Series II has sufficient memory for full-page graphics, the plotting engine is not as good a quality as the original HP Laser Jet that was used for the half-page graphics. A series of full-page complementary contour images of satellite perturbations was prepared, but the white contours were not as easily distinguished. Experiments were then begun with shading the contour map according to sign. Instead of sampling every point as in the complementary contour image and setting the bit according to the sign, every third value was sampled horizontally in every third row and the bit was set according to the sign. This led to the images presented in Ref. 12. The shaded background very nicely joins with the zero contour, and the overall impression is quite pleasing.

This technique is taken two steps further in Fig. 12(a) and 12(b). The surface is sampled in a regular grid by offsetting the evaluation point in a regular 7 × 7 array. A bit is then set if the field value is below a specified amount which divides the total variation of the field into four levels in Fig. 12(a) and into eight levels in Fig. 12(b). The longitude is incremented by 7 pixels through a latitude circle, then the latitude is decremented by 7 pixels from the starting point and the latitude circle then covered. After the whole sphere is covered in this manner, a new field value and starting point in the 7 × 7 array are chosen, and the sphere is again covered by offsetting by 7 pixels in latitude and longitude. Although interesting, the images in Fig. 12 give a feeling of "overkill" in the technique. These images do show that the geoid in Spain lies higher than most of Europe, and other high-low ambiguities are resolved for the unlabeled contours.

Because the grays of Fig. 12 so smoothly join the contour lines, the offsetting technique is extended to the full 50-step gray scale used for Figs. 10(a) and 10(b). The offsets are chosen to give a somewhat uniform fill-in to the fundamental 7 × 7 grid. Although it has been heightened in the reproduction, the original of Fig. 10 is not satisfactory because there is too little contrast (but no worse than some images obtained through the photographic film process). The right track is found. Figures 10(a) and 10(b) look like integrated black and white images, and the contrast of the image can be changed by simply adjusting DO-loop counters. Since a single pixel in Fig. 10 corresponds to 0.15°, there is less detail here than in Rapp's 1/8° data set.

Pixel setting by the offset technique provides unexpected bonuses. In flat areas, a regular pattern of gray-level blocks is formed, just as in Fig. 11. But since the field value is sampled eventually at nearly every point in the graphic, sharp lineations as small as a single bit are represented instead of being either stepped over or given a discontinuous, noisy appearance (as in Fig. 11(b)).

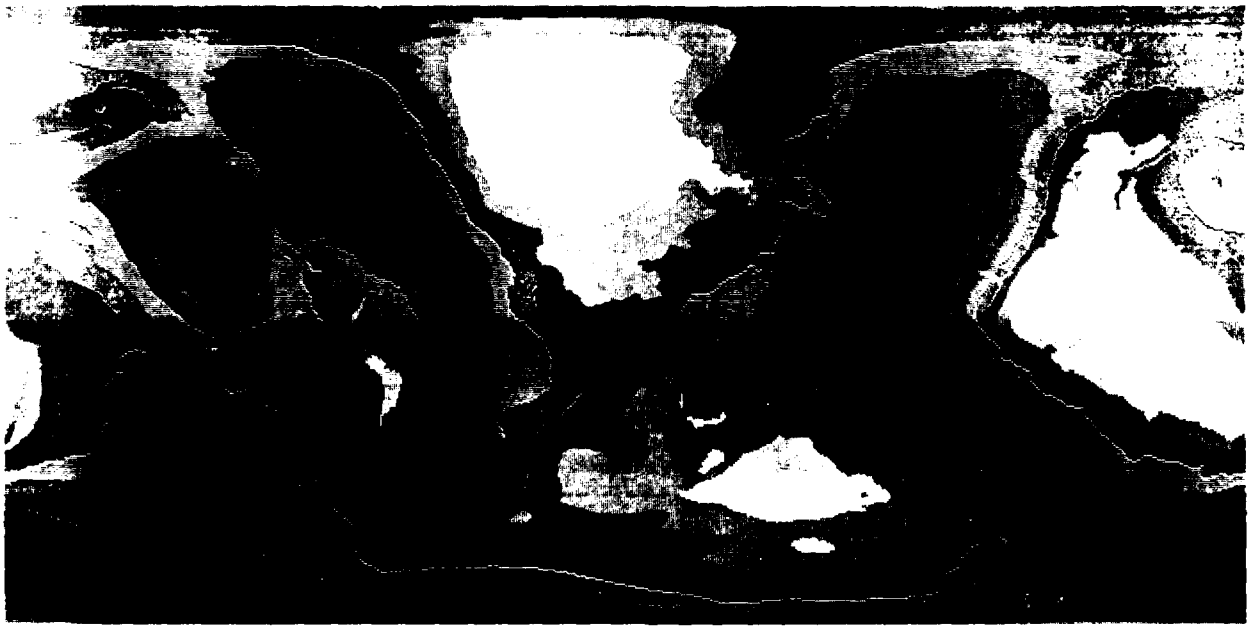

a. Seventeen levels

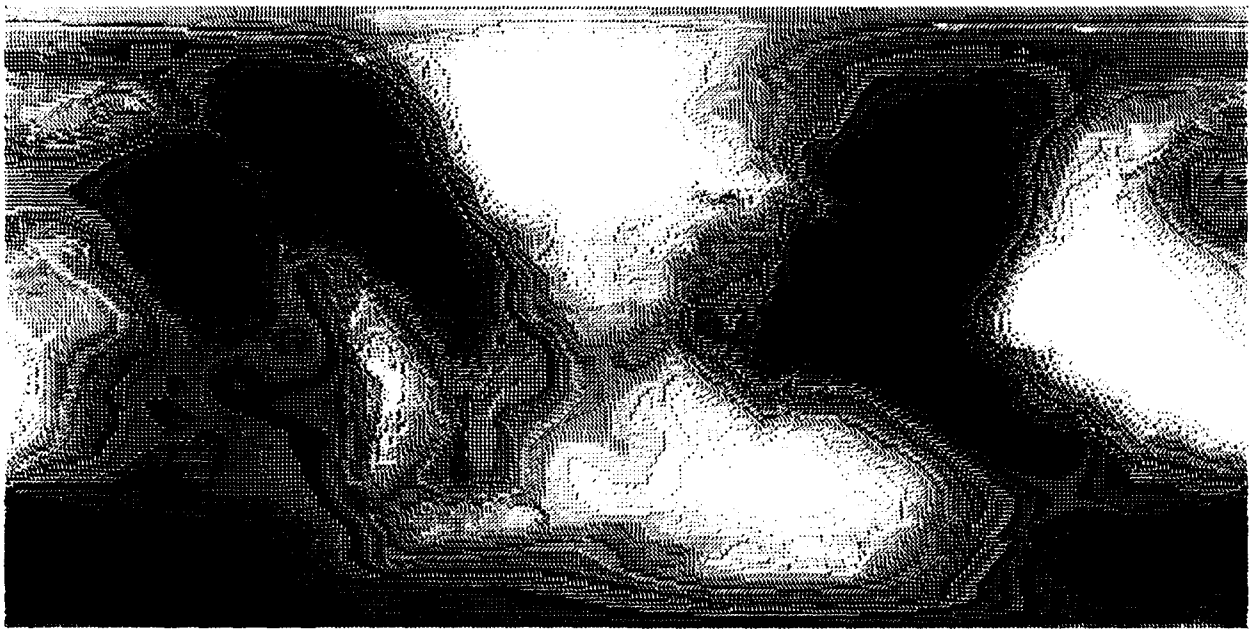

b. Sixty-five levels

Fig. 11 — Gray scale experiments on the undulation

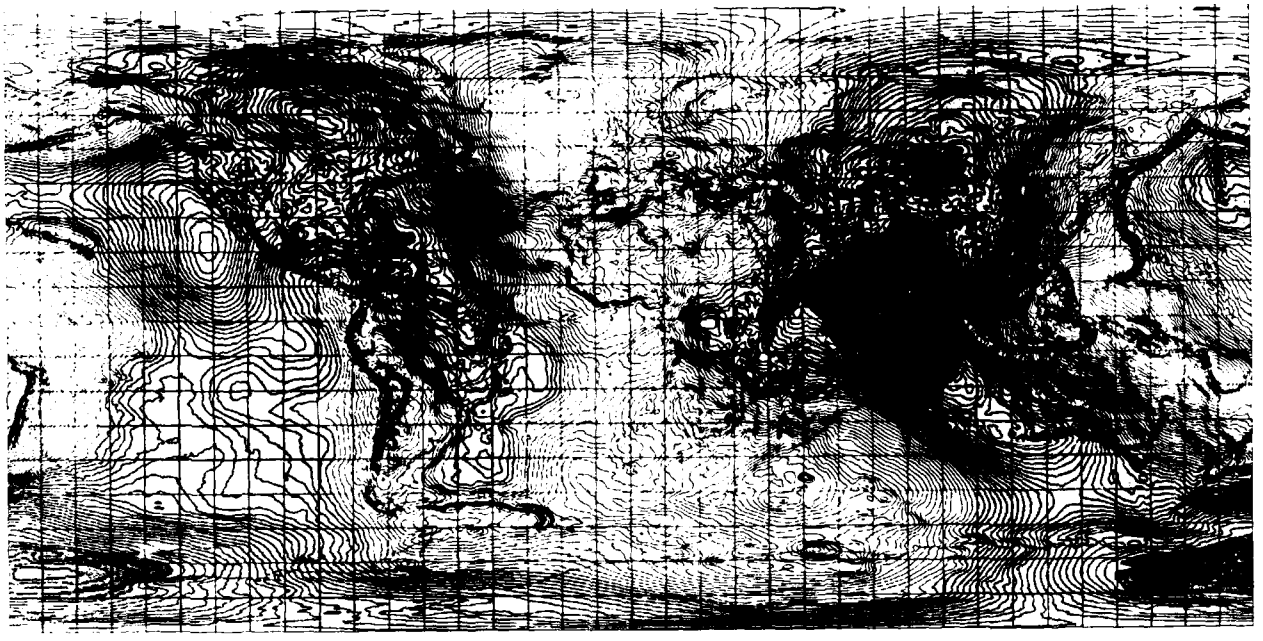

a. Four levels

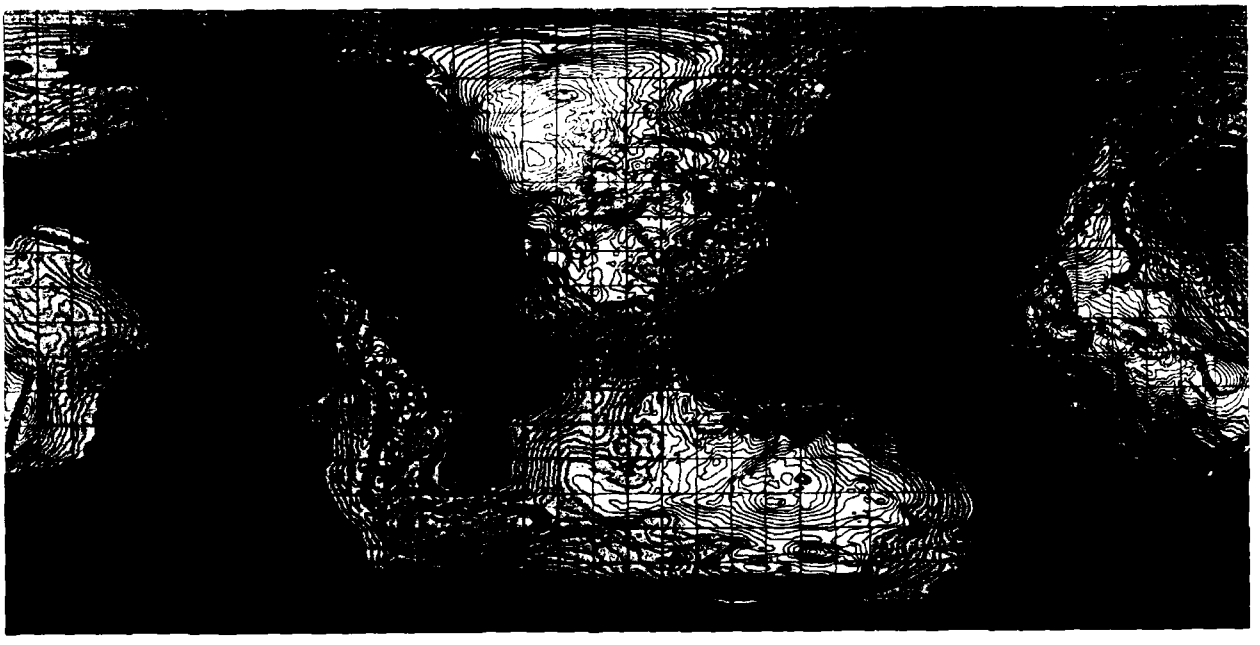

b. Eight levels

Fig. 12 — The undulation of OSU86F

The sampling at every pixel also has a smoothing effect that eliminates the pseudo contour lines (as in Fig. 11(a)). One of the initial goals of developing graphics on dot matrix devices was not met. It had been hoped that it would be possible to copy the original in an ordinary copy machine, but the 300 dot per inch graphics do not copy well because of resolution degradation.

AN ATLAS OF THE 360TH ORDER GEOPOTENTIAL OSU86F

After finding a good method for creating a gray scale, it was decided to go to full-page graphics; these are presented in Figs. 13 through 28. Various contrast experiments were performed. In the originals, the most satisfactory results are obtained by not using the full range of field values. The contrast is improved in Figs. 13 and 14 over 10(a) by using 5-m instead of 4-m gray levels and by going from white but not all the way to black (which leaves detail in the Indian Ocean low). Although the spatial resolution is lower, the images in Figs. 13 through 28 are as good as any the author has produced on high-resolution graphics tubes.

Figures 9(a), 12, 13, and 14 are the undulation of the geoid for OSU86F. The gray scale geoid in Figs. 13 and 14 is presented both with and without the continental outlines to show the surface and then the association of the surface with geography. The changes in the undulation of the geoid are seen by comparing Figs. 1(a) and 9(a) and how well the GEOS-3/SEASAT data are preserved from Fig. 8(a).

The differences in the models become most apparent with the derivative fields. The detail in OSU86F is outstanding. Examination of the maps shows that much more detail is available in the United States, Europe, South Africa, and Australia. In addition for OSU86F, Rapp and Cruz have brought the Gibbs phenomenon, which appears in RAPP81, under control near the very short wavelength features such as the North Pacific trenches, the Puerto Rico trench, and Hawaii. (Until the evaluation of OSU86F, the author was not sure if the "ringing" near these features was due to his evaluator or was in the model coefficients). It is expected that the price paid for the control of the Gibb's phenomenon is the loss of information in other features.

Figures 15 through 20 show the OSU86F gravity disturbance. So many graphics are given of this particular field because it bears the most relation to geophysical features. Successively finer gray levels are used in Figs. 15 through 19. In Fig. 17, a 10 mGal step is used from -200 to 200 mGal, which brings shading to all but the most extreme features. In Fig. 18 the gray level is 2.5 mGal from -50 to 50 mGal. The most pleasing graphic of the gravity disturbance, which is used in the higher resolution images in Figs. 15 and 16, is found for a gray level of 5 mGal from -100 to 100 mGal. In Fig. 19 the gray step is 1 mGal to accentuate the flatter ocean features. In Fig. 20 a variable gray level scheme ($-300, \ldots, 0, 1, 2, 3, 4, 6, 8, 10, 15, 20, 25, 30, 35, 40, 45, 50, 75, 100, 150, 200$, 300 mGal) is used to provide shading information throughout the range of the gravity disturbance, but the graphic contrast is not as pleasing as in Fig. 15.

Figures 21 and 22 show the longitude and latitude deflections with a gray level of 2.5 mGal from -50 to 50 mGal. The author's crude attempts at shaded relief on the undulation of the geoid looked very much like these images.

Figure 23 shows the second radial derivative of the anomalous potential. The gray level is in 0.25 Eötvös steps from -5 to 5 Eötvös units.

The areas where Rapp used geophysical correlation data are very clear in this graphic. Over China the data blocking is apparent. The values in the Soviet Union are the smoothed Defense Mapping Agency (DMA) values. The gravity gradient components in Figs. 24, 25, 26, and 28 use the same gray level scheme. Note also in Figs. 24, 26, and particularly in 27 the very sharp lineation of the gravity gradient components along the Ethiopian coast.

Fig. 13 — OSU86F, undulation of geoid

Fig. 14 — OSU86F, undulation of geoid with map

Fig. 15 — OSU86F, gravity distur

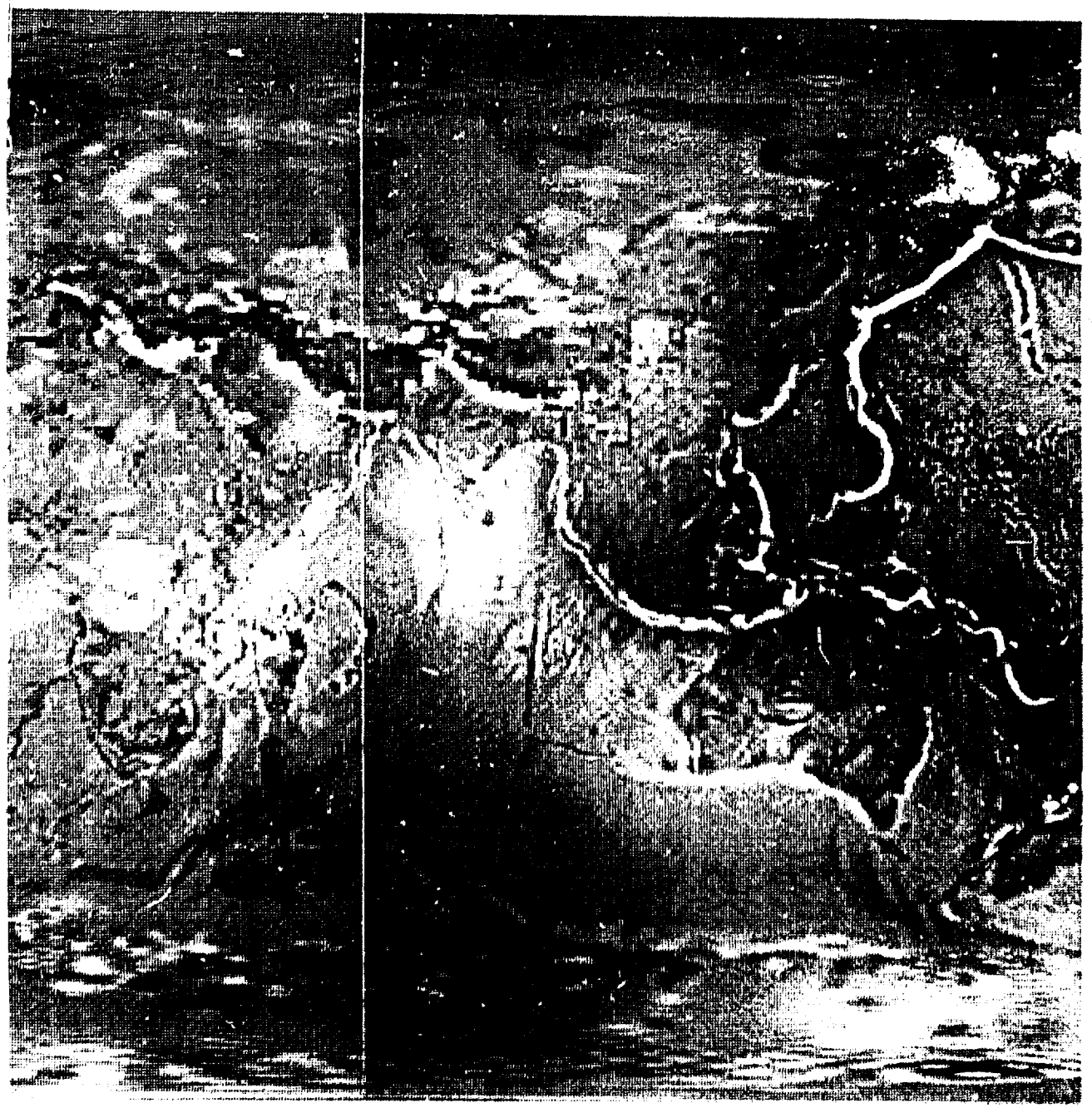

ince. (4th-order geopotential

Figure 27 presents the best comment on the high quality of OSU86F over the oceans. Here the gray level is reduced to 0.1 Eötvös units in the range from -2 to 2 Eötvös. This graphic shows that Rapp and Cruz took care of the ground trace problem that appears in RAPP81.

The quality of OSU86F appears so good and the incremented gray scale method gives such a nice image that a three-panel map of the gravity disturbance was created (Fig. 15). This 3-megabyte graphic at 300 dots per inch contains more information than could be put on the 18 $\times$ 36 in. maps at 200 dots per inch.

Most maps of the gravity field break at the prime meridian. The author prefers to pick longitude values in the symmetrical interval from $-180°$ to $180°$. Figure 16 is provided to give continuity in the gravity disturbance image at $180°$ where the author's maps are usually broken.

Fig. 16 — OSU86F, gravity disturbance

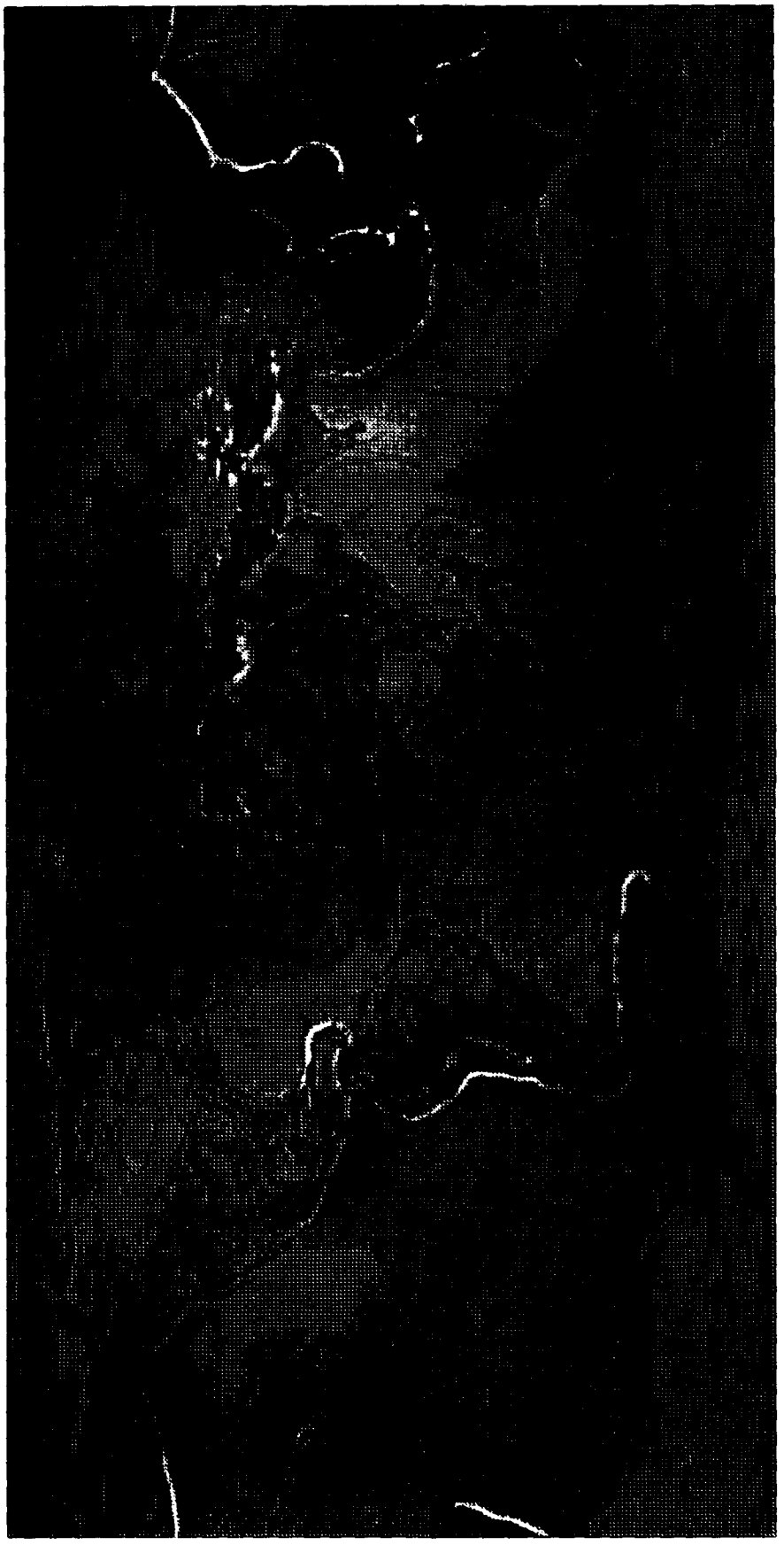

Fig. 17 — OSU86F, gravity disturbance

Fig. 18 — OSU86F, gravity disturbance

Fig. 19 — OSU86F, gravity disturbance

Fig. 20 — OSU86F, gravity disturbance

Fig. 21 — OSU86F, longitude disturbance

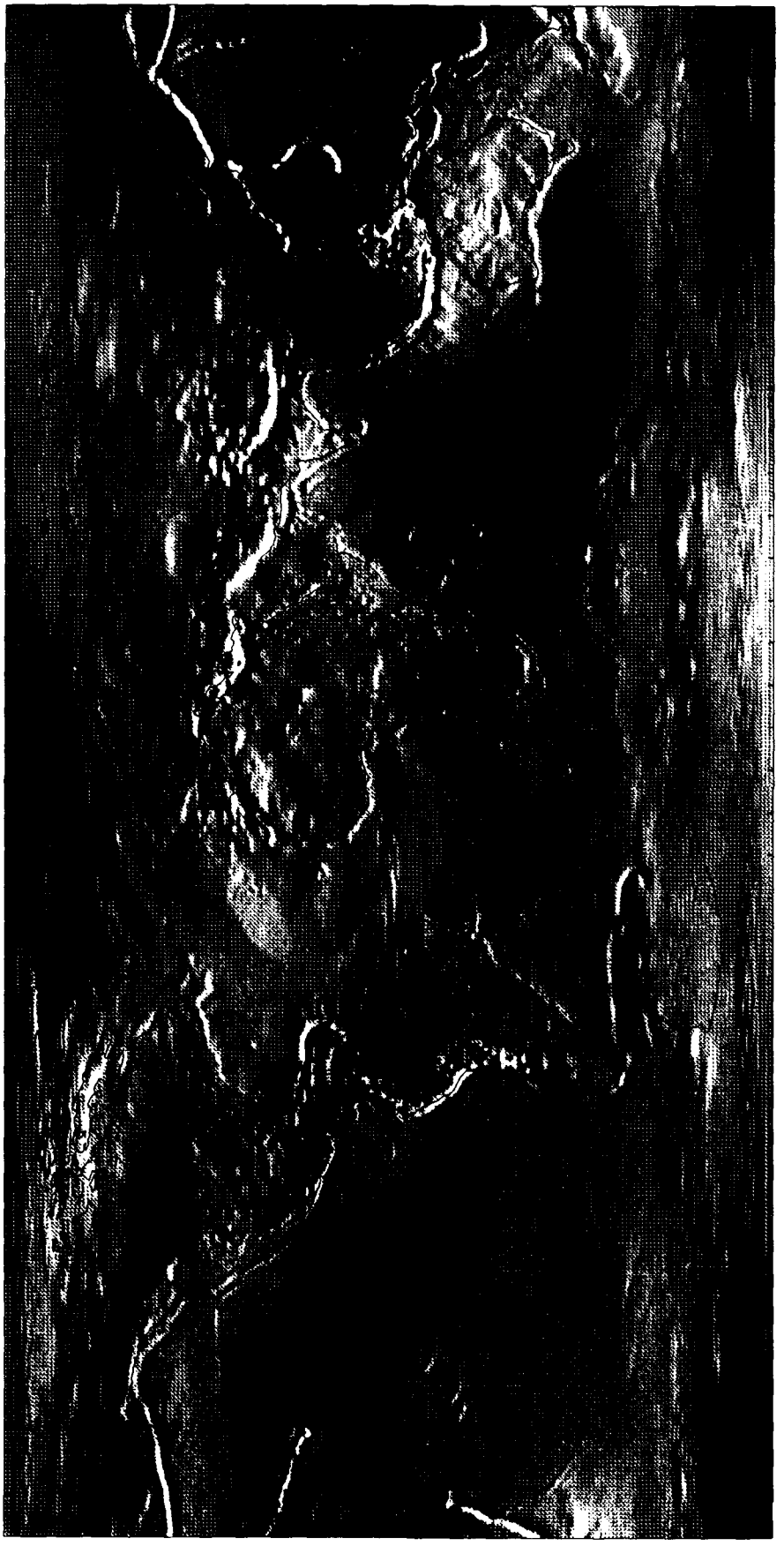

Fig. 22 — OSU86F, latitude disturbance

Fig. 23 — OSU86F, radial-radial gravity gradient

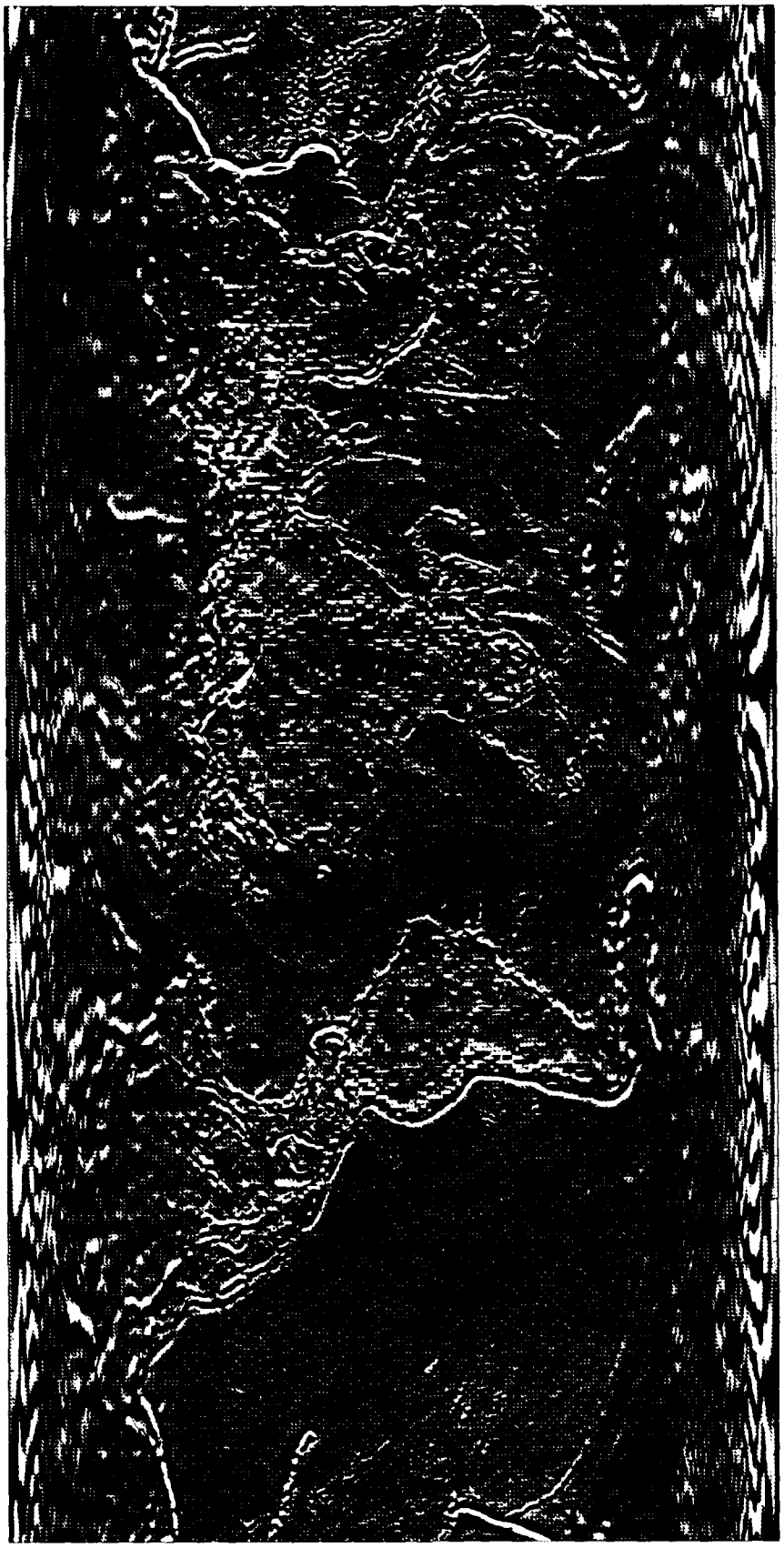

Fig. 24 — OSU86F, radial-longitude gravity gradient

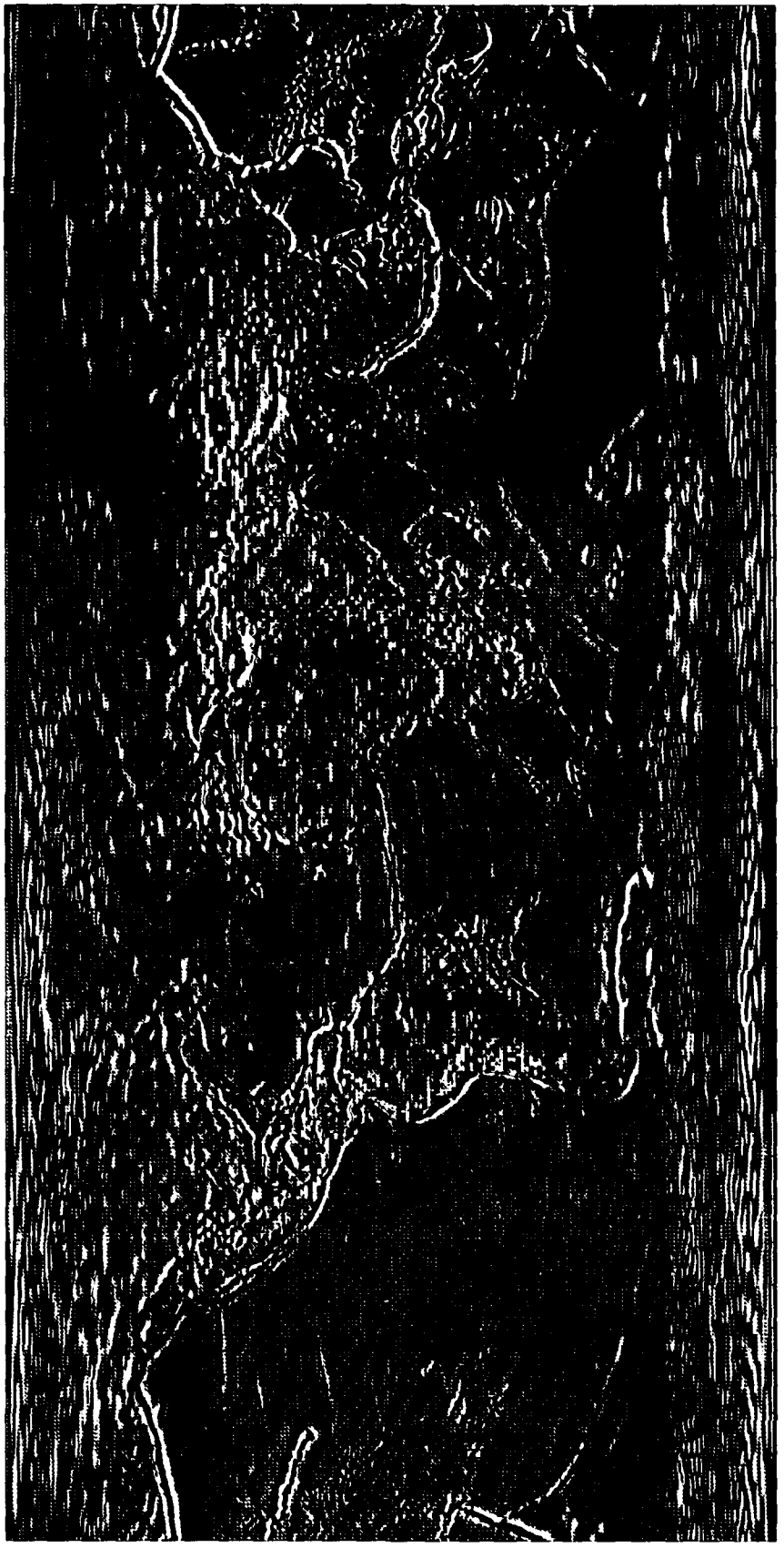

Fig. 25 — OSU86F, radial-latitude gravity gradient

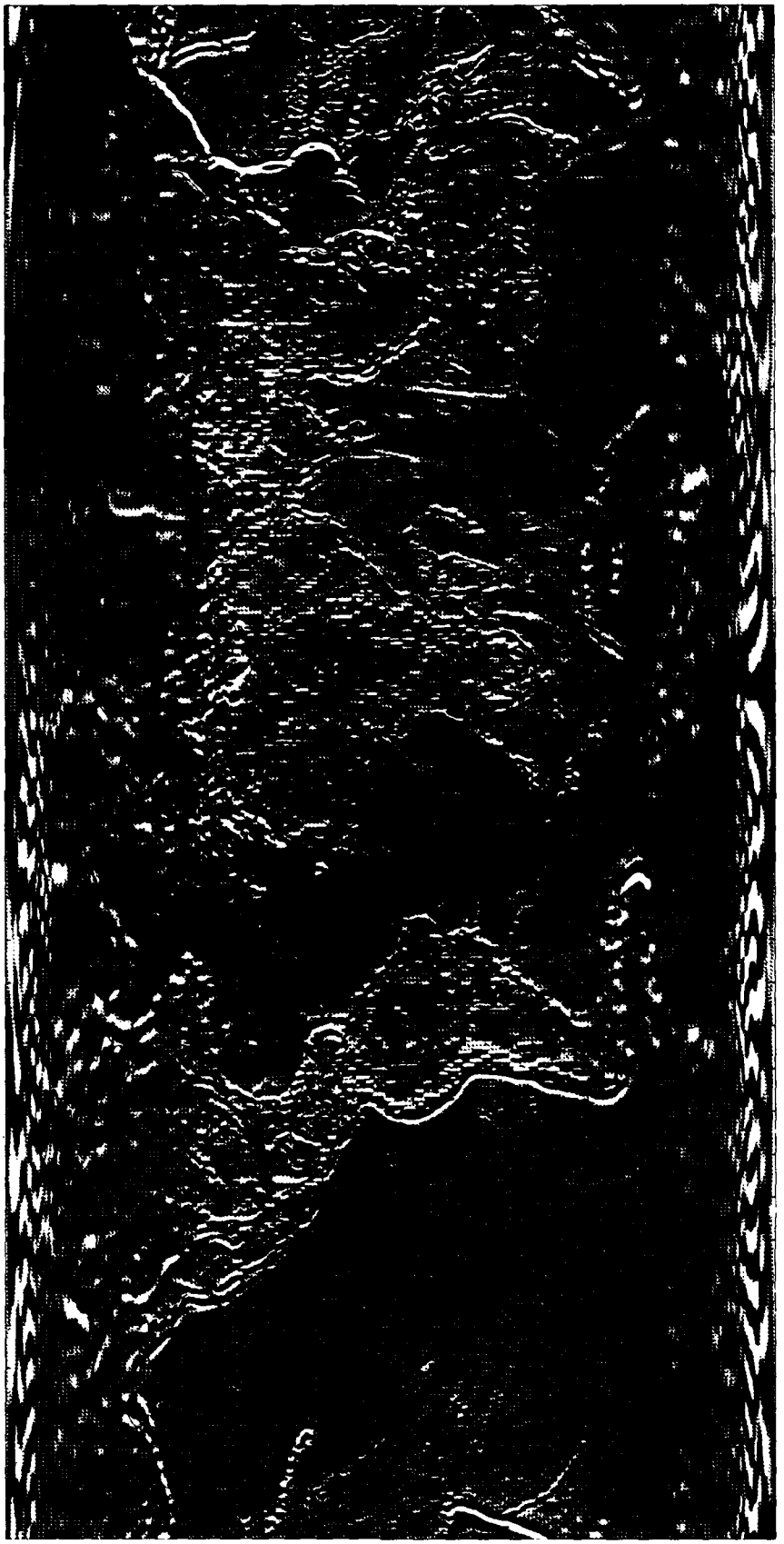

Fig. 26 — OSU86F, longitude-longitude gravity gradient

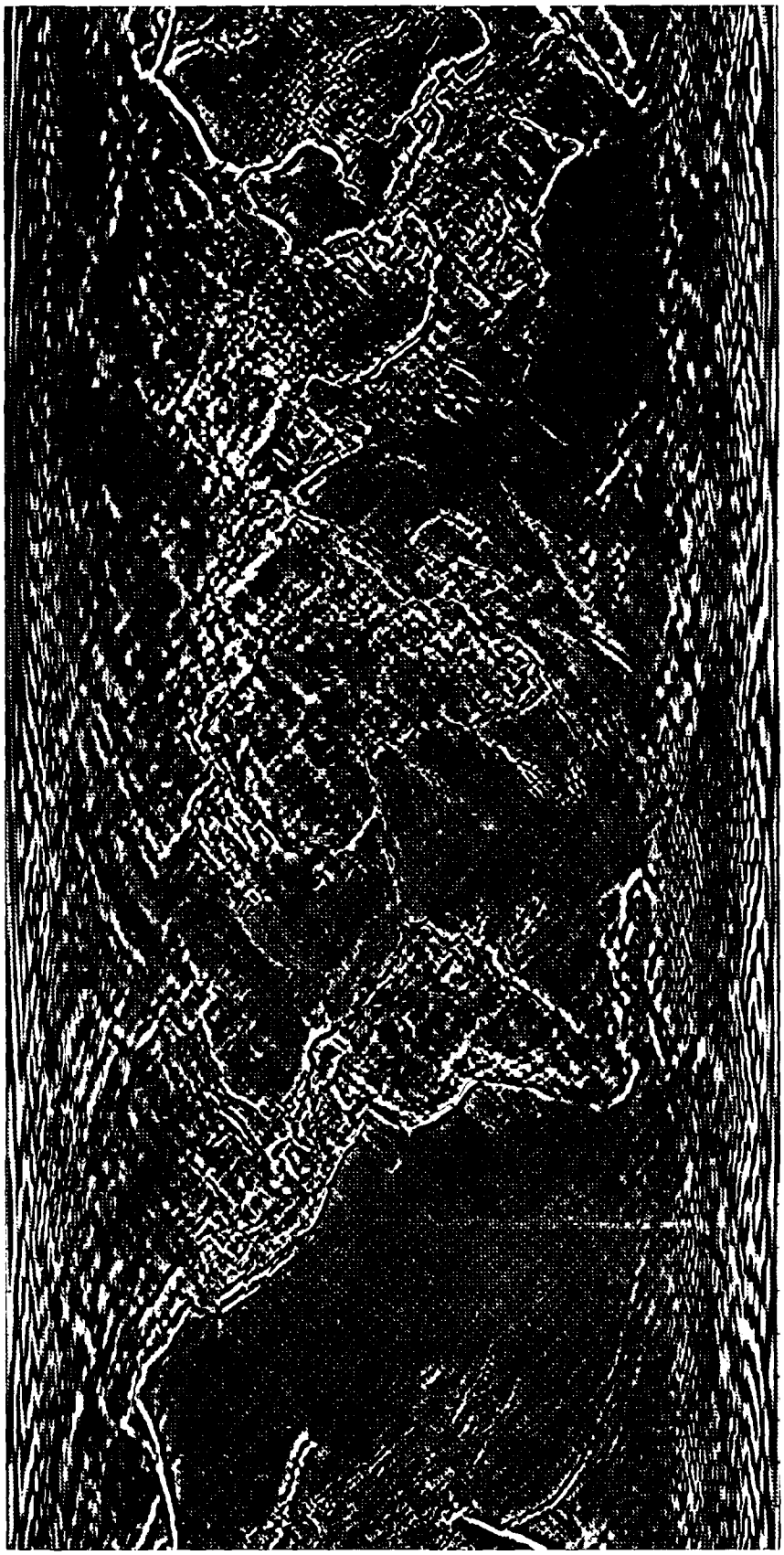

Fig. 27 — OSU86F, longitude-latitude gravity gradient

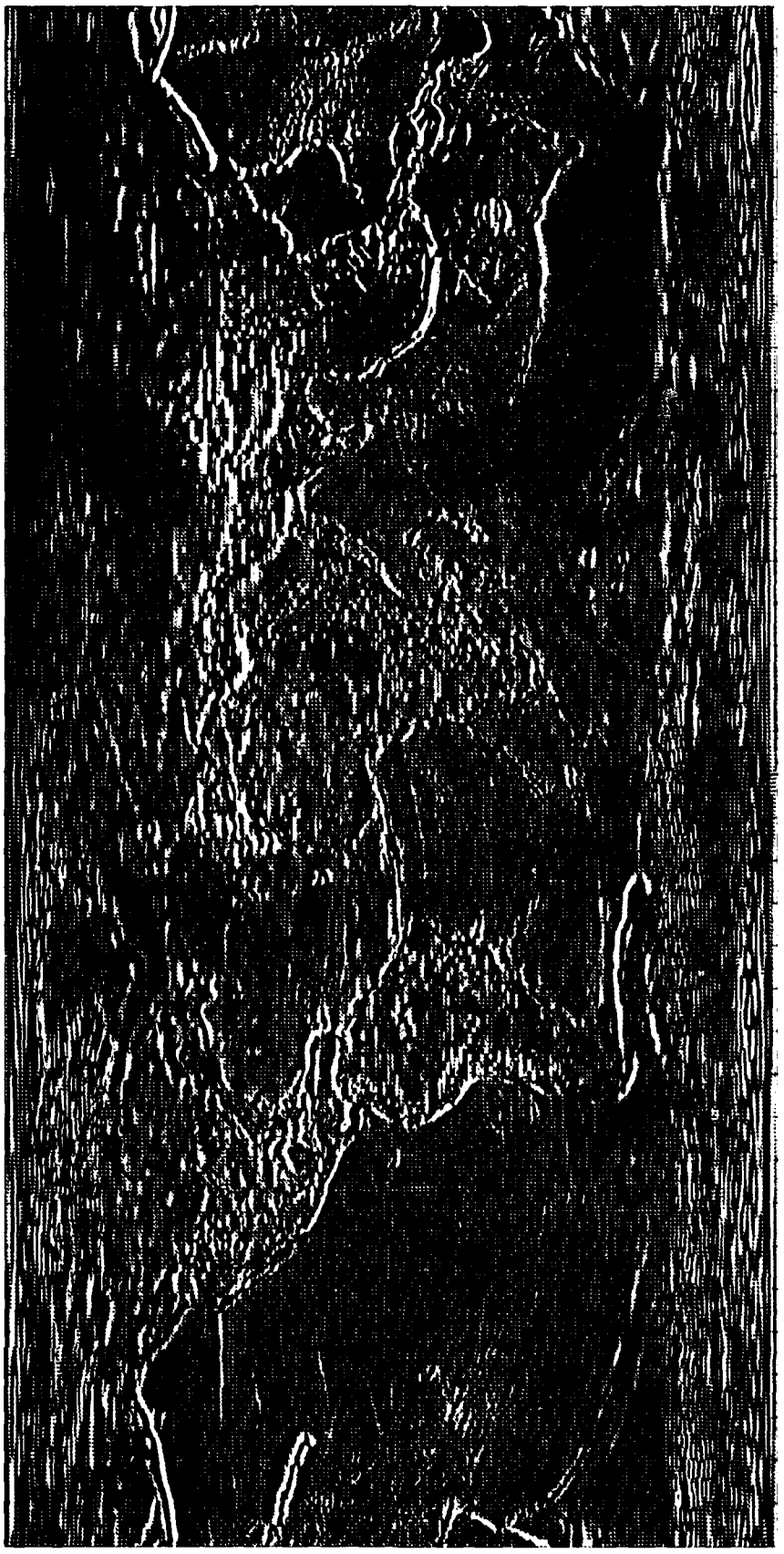

Fig. 28 — OSU86F, latitude-latitude gravity gradient

SPHERICAL PROJECTIONS

The equal angle projection is preferred for the presentation of gravity data because it is both the most common mode and because the whole world is represented in a single graphic. Others prefer the geometrical insight provided by a spherical projection. Figure 29 gives four images of the undulation of the geoid for OSU86F. The initial idea was to produce stereo pairs, but the stereo images were disappointing. The spherical images are so distinctive that they are included in this report. A 1° grid is used over most of the globe, but it becomes so crowded near the pole that only the latitude grid is used at latitudes greater than the SEASAT inclination. A similar graphic was made by using SEASAT ground traces for the grid, but the results were not as satisfactory.

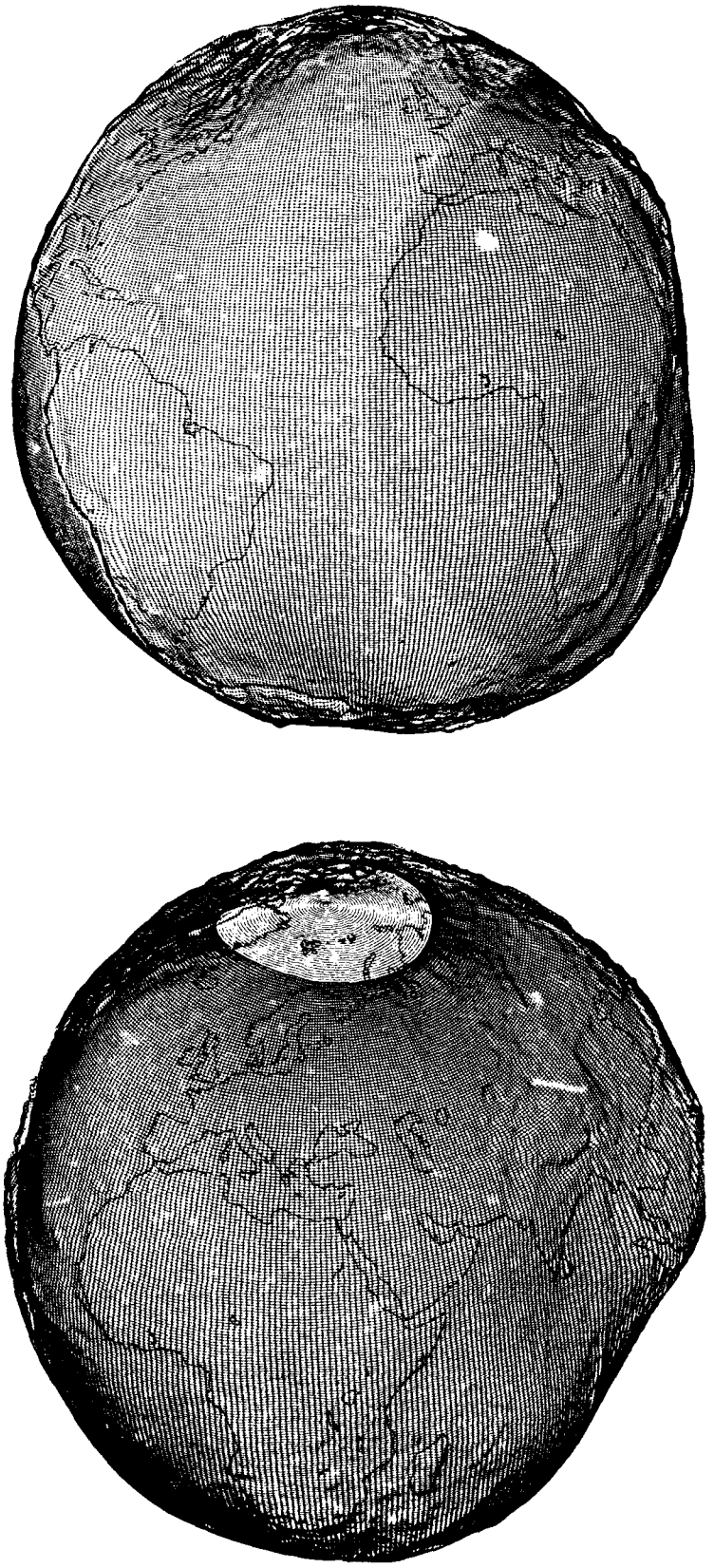

Fig. 29 — OSU86F, undulation of geoid

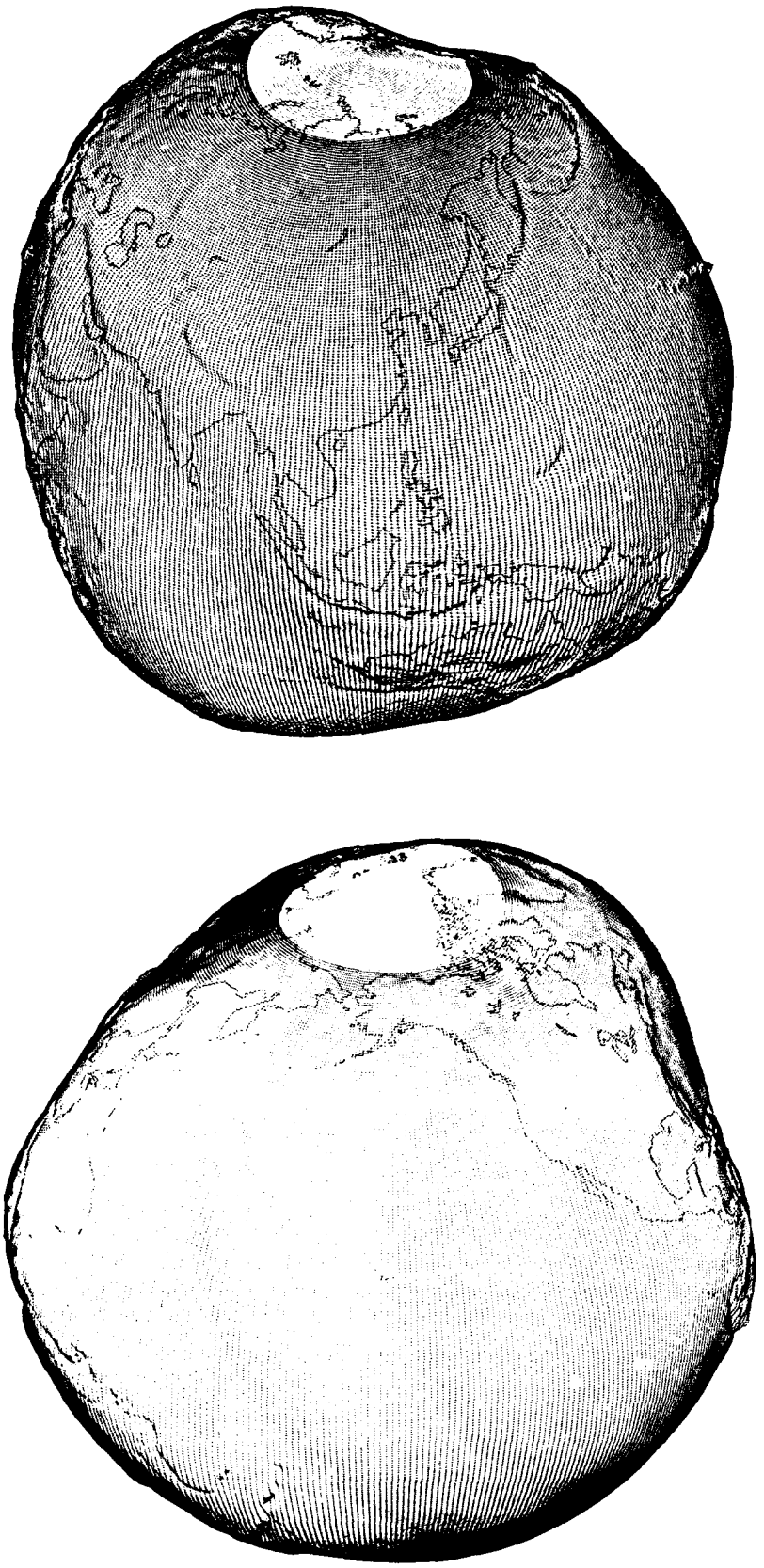

Fig. 29 (Cont'd) — OSU86F, undulation of geoid

COMPARISON OF LOW-ORDER MODELS

One of the frustrations in developing the large scale maps reported in Ref. 5 was the use of a commercial, device-independent, graphics software package. The original contouring algorithm was developed on a 16K computer as described in Ref. 1, and the vectors that make up the contour map are not stored but are plotted immediately. Versatec plotters require that all vectors be stored before plotting. For the force components, the limit of VAX virtual memory is easily reached with a resulting system crash. With the plotting package developed at NRL, the graphic is formed as a bit image in memory. This technique means that the same amount of memory (which changes with the overall size) is used for each graphic.

The initial development of the plotting package in the spring of 1986 coincided with the release to the author of the WGS84 Earth Gravity Model, see Macomber [16], Decker [17], and White [18]. Although WGS84 is now unclassified to order 18 (see Smith [19]), at the time only order 12 was unclassified. Figures 30 to 32 were presented at the 1986 Spring American Geophysical Union meeting in Baltimore, see Ref. 20, as a blink comparison on the HP IPC. In this comparison, each of the 12th order fields from WGS84, GEM-L2 of Lerch et al. [21], and RAPP81 was rapidly brought to the screen of the computer. With the availability of 180th and 360th order models, it might be naively thought that the low-order geopotential models are well defined. On the computer screen the contour lines wiggled in a manner reminiscent of a bowl of gelatin. Readers can judge for themselves by quickly flipping the pages to intercompare the three models.

In Figs. 30(a), 31(a), and 32(a) the undulation of the geoid is plotted with a contour interval of 5 m. In parts (b) through (d) of Figs. 30 through 32 the three components of the anomalous gravitational force for the three models are plotted with a contour interval of 5 mGal. Each of the 12 maps is a screen dump on the HP IPC's built-in printer and represent 16K of memory. A toggle on the HP IPC allows for changing the monochrome screen from black letters on a white background to white letters on a black background, which is equivalent to complementing each bit that makes up the screen. This feature led to the development of the "complementary contour images."

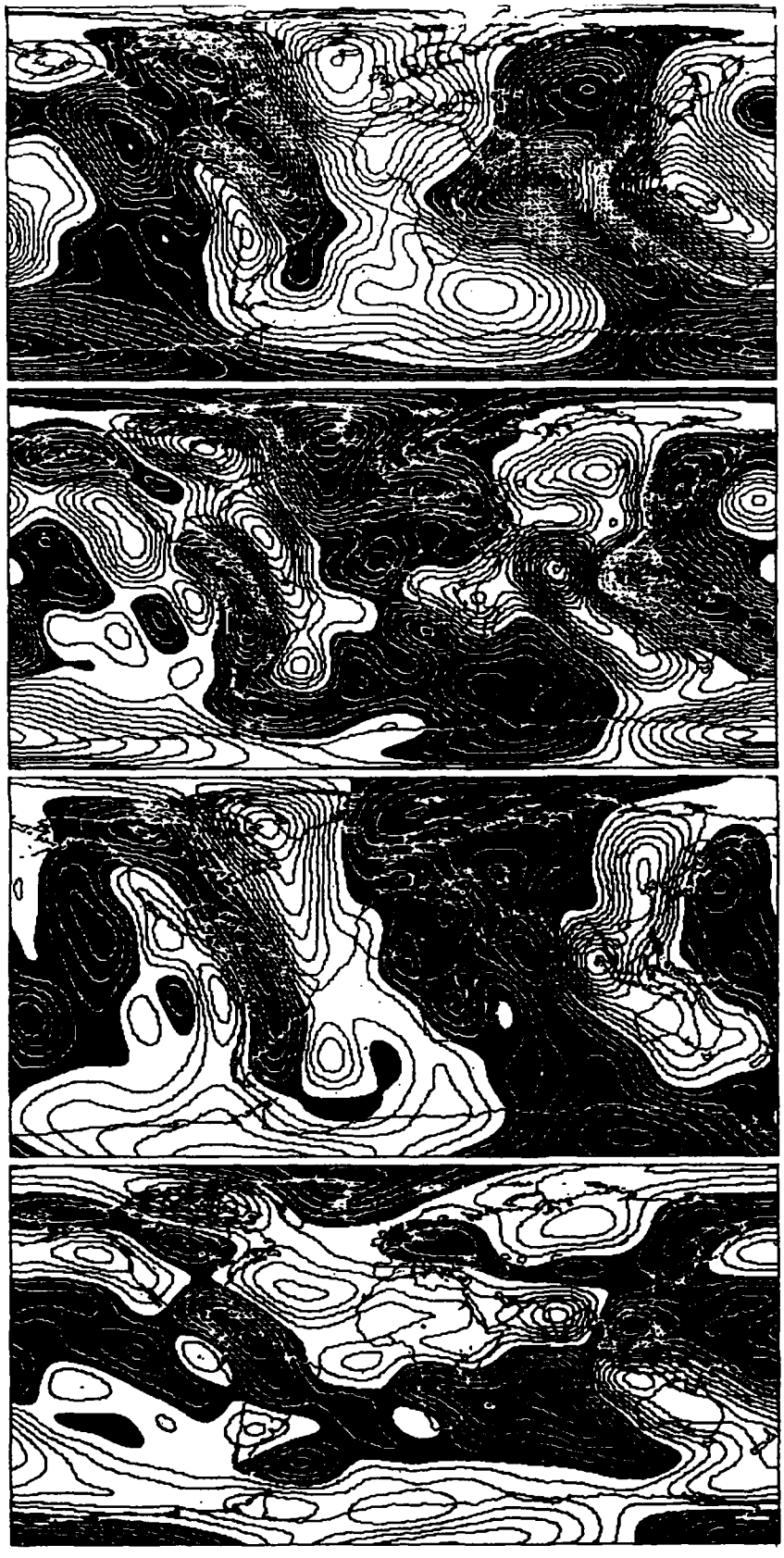

a. Undulation of geoid

b. Gravity disturbance

c. Longitude disturbance

d. Latitude disturbance

Fig. 30 — Fields derived from WGS84 at order 12

ON ALGORITHM VALIDATION

The author first validated the Legendre polynomial summation algorithms in 1983 by comparing the undulation of the geoid for GEM10B with that in Ref. 2 (see Figs. 1 and 2 of Ref. 1). The location of contours is sufficiently sensitive that it eliminates all but very subtle errors. An additional problem is that each derivative of the geopotential is a different series and as such must be independently validated. Really, two issues are involved. The first is the summation of the full series to obtain the geopotential, the three gravitational force components and the five independent Hessian components; the second is the conventions used to eliminate the major terms caused by the ellipsoid and the formulas used to represent the anomalies. The first problem is mathematical; the second is geodetic convention.

The issue of algorithm validation was not revisited until the spring of 1986. There was a requirement to have a geopotential algorithm for computing satellite orbits beyond order 25 where the unnormalized algorithm due to DeWitt [22] would no longer work on the VAX because of the exponent overflow described in Ref. 5. Double-precision agreement to 16 decimals was obtained between the author's and DeWitt's algorithms for the gravitational force of the 12th order WGS84 model for a point in inertial space. In seeing such agreement, one comes to the quasi-mystical realization that the mathematical summation of Legendre polynomials with the same set of coefficients must yield the same value. This exercise validated the computation of the three-force component series.

The author has no plans to produce his own spherical harmonic model, and B. Louis Decker of the Defense Mapping Agency noted in a conversation that it is unlikely a new WGS model will be produced before the next century. The motivations for this work are the insights provided by the images and the intellectual thrill of seeing the detail of the high-order models. Also, a single researcher with a computer and plotter and guided by mathematical rules can see the work of hundreds of geodesists who patiently compiled the gravity data and the results of millions of dollars in government satellites.

ACKNOWLEDGEMENTS

Professor Rapp is thanked for the marvelous data sets. The plotting package was developed by Matthew R. Singer now with the MIT Lincoln Laboratories. It was only through Singer's persistence that the mass of data on the 1/8° tapes was moved to disk and separated into files. Robert R. Dasenbrock of NRL developed the spherical projection software.

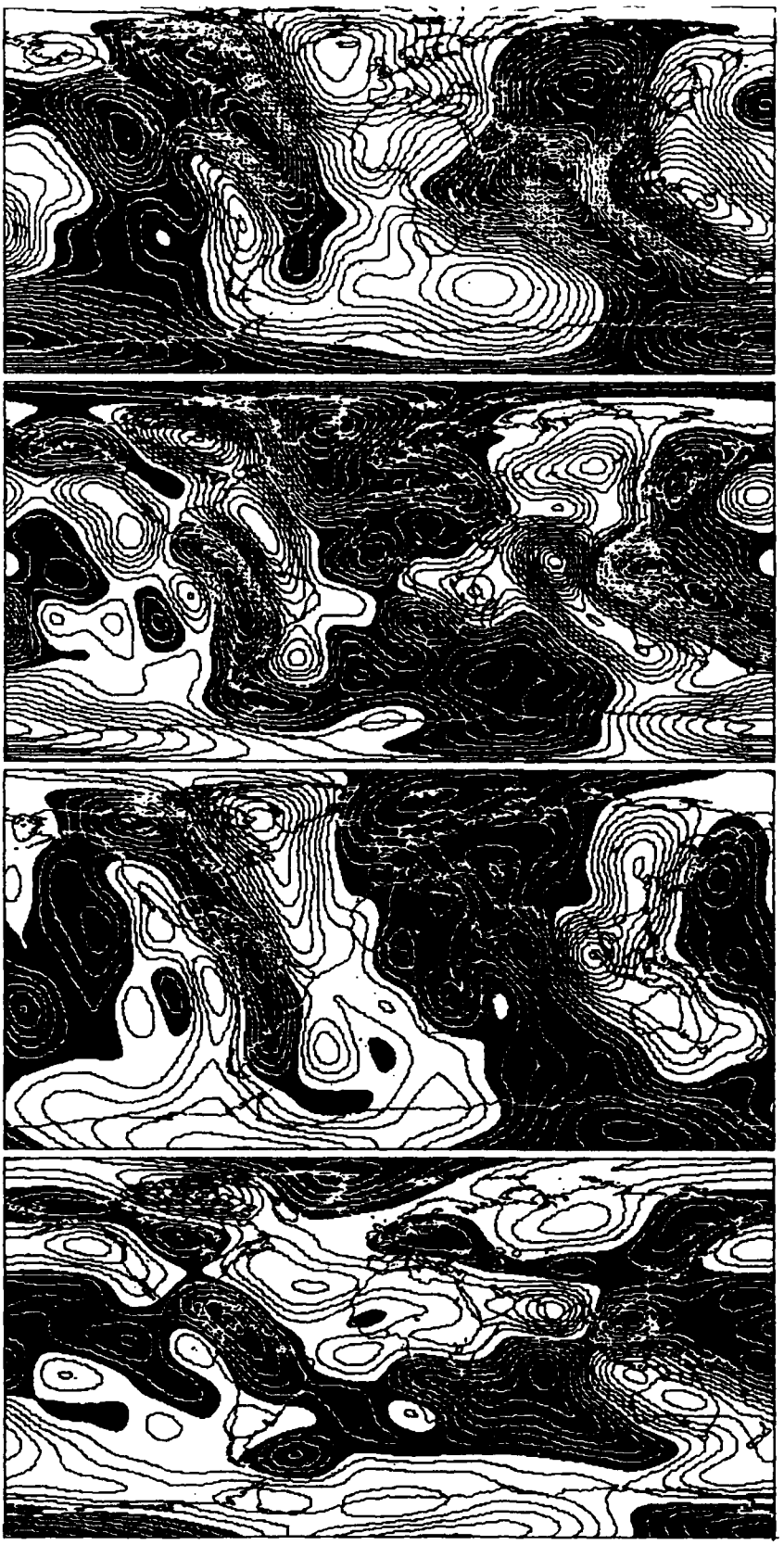

a. Undulation of geoid

b. Gravity disturbance

c. Longitude disturbance

d. Latitude disturbance

Fig. 31 — Fields derived from GEM-L2 at order 12

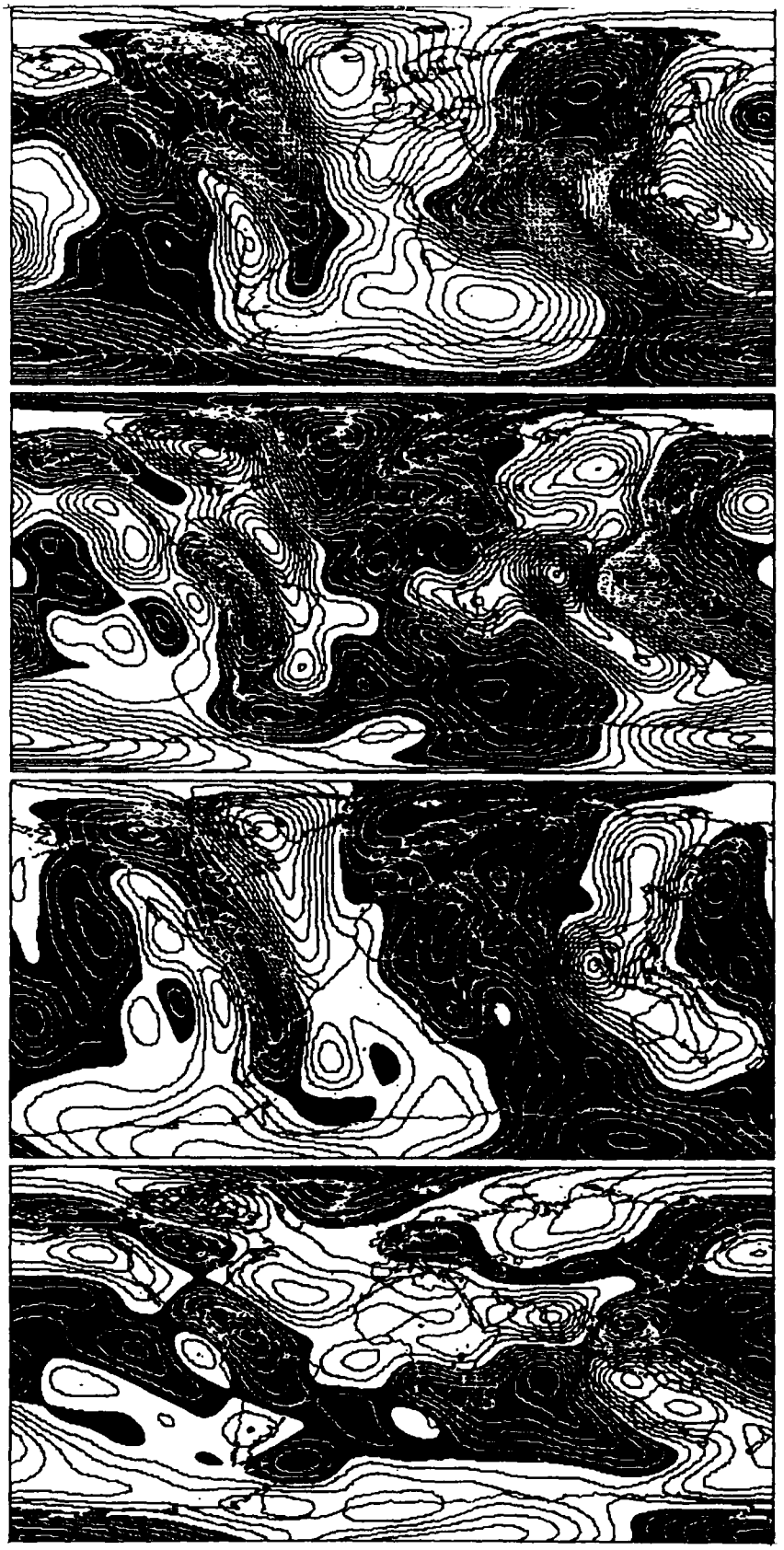

a. Undulation of geoid

b. Gravity disturbance

c. Longitude disturbance

d. Latitude disturbance

Fig. 32 — Fields derived from RAPP81 at order 12

REFERENCES

1. P.J. Melvin, "The Computation of Anomalous Gravity from Spherical Harmonic Expansions," Boeing Document No. D180-27964-1, 1984; see also *EOS* **65**(16) (1984).

2. F.J. Lerch, B.H. Putney, C.A. Wagner, and S.M. Klosko, "Goddard Earth Models for Oceanographic Applications (GEM10B and 10C)," *Marine Geodesy* **5**(2), 145 (1981).

3. P.J. Melvin, "Poisson Series Solution of Geosynchronous Drift," AIAA 83-0016, AIAA 21st Aerospace Sciences Meeting, Reno, NV, 1983.

4. F.J. Lerch, S.M. Klosko, R.E. Laubscher, and C.A. Wagner, "Gravity Model Improvement Using GEOS 3 (GEM9 and 10)," *J. Geophys. Res.* **84**(B8), 3897-3916 (1979).

5. P.J. Melvin, "Comments on the Summations of Spherical Harmonics in the Geopotential Evaluation Theories of Deprit and Others," *Celestial Mechanics* **35**, 345-355 (1985).

6. R.H. Rapp, "The Earth's Gravity Field to Degree and Order 180 Using SEASAT Altimeter Data, Terrestrial Gravity Data, and Other Data," Report No. 322, Department of Geodetic Science, The Ohio State University, 1981.

7. P.J. Melvin, "An Atlas of Rapp's 180th Order Geopotential" (AAS 85-333), *Astrodynamics 1985*, Vol. 58, Part 1, *Advances in the Astronautical Sciences*, Kaufman, Liu, Calico, and Hoots, eds. Proc. AAS/AIAA Astrodynamics Specialist Conference, Vail, CO, Aug. 1985 (Univelt, San Diego, CA, 1986), pp. 677-696.

8. R.H. Rapp, "Detailed Gravity Anomalies and Sea Surface Heights Derived from GEOS-3/SEASAT Altimeter Data," Report No. 365, Department of Geodetic Science, The Ohio State University, 1985.

9. R.H. Rapp, "Gravity Anomalies and Sea Surface Heights Derived from a Combined GEOS-3/SEASAT Altimeter Data Set," *J. Geophys. Res.* **91**(B5), 4867-4876 (1986).

10. R.H. Rapp and J.Y. Cruz, "Recent High Degree Expansions of the Earth's Gravitational Potential," *EOS* **67**(44), 909 (1986); see also Report No. 376, Department of Geodetic Science, The Ohio State University, 1986.

11. P.J. Melvin, "Spectral Analyses of Satellite Geopotential Missions," Presented at the Chapman Conference on Progress in the Determination of the Earth's Gravity Field, Ft. Lauderdale, FL, 1988.

12. P.J. Melvin, "Satellite Geodesy from Orlov's Plane" (AAS 87-536), *Astrodynamics 1987*, Vol. 65, *Advances in the Astronautical Sciences*, Soldner, Misra, Lindberg, and Williamson, eds., Proc. AAS/AIAA Astrodynamics Specialist Conference, Kalispell, MT, Aug. 1987 (Univelt, San Diego, CA, 1988) pp. 1449-1472.

13. P.J. Melvin, "The Figure-of-8 Librations of the Gravity Gradient Pendulum and Modes of an Orbiting Tether: II. Geodetic, Mass Distribution and Eccentricity Effects," AIAA 88-4283-CP, AIAA/AAS Astrodynamics Conference, Minneapolis, MN, 1988.

14. P.J. Melvin, "Maps of Rapp's 180th Order Geopotential," *EOS* **66**(18) (1985).

15. Geodynamic Map of the Circum-Pacific Region, American Association of Petroleum Geologists, Tulsa, OK, 1986.

16. M.M. Macomber, "World Geodetic System 1984," Defense Mapping Agency, 1984.

17. B.L. Decker, "World Geodetic System 1984," Proc. Fourth International Geodetic Symposium on Satellite Positioning, Co-Sponsors Defense Mapping Agency and National Geodetic Survey, Austin, TX, Vol. 1, pp. 62-92, 1986.

18. H.L. White, "The World Geodetic System 1984 Earth Gravitational Model," Proc. Fourth International Geodetic Symposium on Satellite Positioning, Co-Sponsors Defense Mapping Agency and National Geodetic Survey, Austin, TX, Vol. 1, pp. 93-116, 1986.

19. R.W. Smith, "Department of Defense World Geodetic System 1984—Its Definition and Relationships with Local Geodetic Systems," Defense Mapping Agency, DMA TR 8350.2, Second Printing, 1987.

20. P.J. Melvin, "An Algorithm for On-board Gravity Compensation," *EOS* **67**(16), 261 (1986).

21. F.J. Lerch, S.M. Klosko, G.B. Patel, and C.A. Wagner, "A Gravity Model for Crustal Dynamics (GEM-L2)," *J. Geophys. Res.* **90**(B11), 9301-9311 (1985).

22. R.N. DeWitt, "Derivatives of Expressions Describing the Gravitational Field of the Earth," U.S. Naval Weapons Laboratory, Tech. Memorandum K-35/62, 1962.

23. R.H. Rapp, "A FORTRAN Program for the Computation of Gravimetric Quantities from High Degree Spherical Harmonic Expansions," Report No. 334, Department of Geodetic Science, The Ohio State University, 1982.